

Alma Mater Studiorum Università di Bologna
Archivio istituzionale della ricerca

Geodetic measurements to control a large research infrastructure: The Virgo detector at the European Gravitational Observatory

This is the final peer-reviewed author's accepted manuscript (postprint) of the following publication:

Published Version:

Marsella M., Nardinocchi C., Paoli A., Tini M.A., Vittuari L., Zanutta A. (2020). Geodetic measurements to control a large research infrastructure: The Virgo detector at the European Gravitational Observatory. MEASUREMENT, 151, 1-14 [10.1016/j.measurement.2019.107154].

Availability:

This version is available at: <https://hdl.handle.net/11585/752692> since: 2020-03-23

Published:

DOI: <http://doi.org/10.1016/j.measurement.2019.107154>

Terms of use:

Some rights reserved. The terms and conditions for the reuse of this version of the manuscript are specified in the publishing policy. For all terms of use and more information see the publisher's website.

This item was downloaded from IRIS Università di Bologna (<https://cris.unibo.it/>).
When citing, please refer to the published version.

(Article begins on next page)

1 Geodetic measurements to control a large research 2 infrastructure: the Virgo detector at the European 3 Gravitational Observatory

4 Maria Marsella¹, Carla Nardinocchi^{1,*}, Andrea Paoli², Maria Alessandra Tini³, Luca Vittuari³,
5 Antonio Zanutta³

6 ¹ DICEA-Survey Lab, Università di Roma "La Sapienza", Italy

7 ² EGO - European Gravitational Observatory, Pisa, Italy

8 ³ DICAM, Università di Bologna Italy

9
10 * Correspondence: carla.nardinocchi@uniroma1.it

11 Academic Editor: name

12 Received: date; Accepted: date; Published: date

14 **Abstract:**

15 The Advanced Virgo (AdV) detector is a 3 km long arms Michelson interferometer for gravitational
16 waves detection. The management of a complex and large research infrastructure requires high-
17 precision geodetic surveying for positioning and rearrangement of instruments.

18 This paper describes the establishment of Virgo Reference System (VRS) consisting in a wide-scale
19 high precision geodetic network based on GPS and Total Station measurements, that support the
20 positioning and the alignment of the different elements forming the interferometer. Ground
21 settlement monitoring is strictly required to verify and adapt the interferometer vertical alignment
22 in presence of a steady subsidence process due to infrastructures overloads. The paper describes
23 also the monitoring activity conducted over the years by means of periodic high precision levelling,
24 that was compared with the results with those obtained using differential interferometry based on
25 satellite Synthetic Aperture Radar (SAR) data

26 **Keywords:** monitoring; surveying; interferometer; DInSAR; large research infrastructure; ground
27 settlements; control network.

28

29 **1. Introduction**

30 The Virgo detector located at the site of the European Gravitational Observatory (EGO), in the
31 countryside near Pisa, Italy (Figure 1) [<http://www.virgo-gw.eu/>] is a Michelson laser interferometer
32 formed by two orthogonal 3 kilometres long arms. Multiple reflections between mirrors located at
33 the extremities of each arm extend the effective optical length of each arm to over 300 kilometres. In
34 order to measure distance changes smaller than 10^{-18} m, the laser beams run inside two Ultra-High
35 Vacuum (UHV) pipes hosted in the arms and the test masses (that is the mirrors reflecting the laser
36 beams) are stabilized by huge anti-seismic dampers, located inside vacuum enclosures.

37 The scientific payloads are hosted in three main experimental buildings, named Central Building
38 (CB), North End Building (NEB) and West End Building (WEB).

39 The two orthogonal arms 3 km each are constituted by two resonant cavities delimited by the of
40 relevant suspended mirrors NI-NE (North Input – North End) and WI-WE (West Input – West End).
41 Both the civil structures (perfectly isostatic Gerber beams) and the supporting system of the vacuum
42 tubes, was designed to absorb differential settlements and to carry out realignment operations.
43 Currently, the periodic monitoring campaigns and the module re-alignments are based on traditional
44 surveying. More recently, a remote differential monitoring system (Hydrostatic Levelling System,
45 HLS) is adopted to support the micrometric realignment system (Fig. 10). This system is installed at

46 the most critical points, the Link Tunnel-End Buildings N200-N201 and W200-W201, and provide
47 results that are perfectly consistent with the leveling ones. DInSAR would integrate the routine
48 measurements that should be based primarily on levelling measurements considering the very
49 stringent accuracy requirements.
50



51
Figure 1. Aerial view of Virgo Site.

52 The range of frequency of the detector (from 10 to 6,000 Hz) and its very high sensitivity are
53 designed in order to allow the detection of gravitational radiation produced by supernovae and
54 coalescence of binary systems in the Milky Way and in outer galaxies. The whole interferometer
55 attains optical perfection and is extremely well isolated from the rest of the world in order to be only
56 sensitive to the gravitational waves. To achieve the required sensitivity, involved scientists have
57 developed the most advanced techniques in the field of high power ultra-stable lasers, high
58 reflectivity mirrors and seismic isolation. Comparable efforts are required to implement a reliable
59 procedure to control along the time the position and alignment of the structures and the detector
60 components based on high precision surveying procedures. Therefore, the high accuracy for the
61 levelling is required to control the relative settlement between each couple of vacuum tube support
62 and to keep the stress induced on the welding lips of the tube modules under defined limits.
63 Moreover, for optical reason, the whole interferometer has to be kept in a plane defined by the
64 position of the Beam Splitter mirror and by all the other suspended mirrors (Test Masses).

65 The Virgo project obtained the scientific goal to meet the sensitivity requirements during the
66 years 2003÷2010 and in 2011 it has received the approval for carrying out an upgrading to further
67 enhance its sensitivity. In 2012, started the construction of Advanced Virgo (AdV) [1], upgraded
68 configuration of the interferometer. AdV was designed to improve the sensitivity by a factor 10, thus
69 allowing the observation of a volume of Universe 1000 times larger. Advanced Virgo together with
70 the other Gravitational Waves (GW) detectors running in their upgraded configuration (Advanced
71 LIGO - USA, GEO600 – Germany, KAGRA - Japan) is part of the network designed for the
72 contemporary detection of the signals coming from the Universe, which will start the era of the GW
73 Astronomy.

74 After the first detection of a gravitational wave signal with ground interferometers made by
75 Advanced LIGO in September 2015 [2], recently Advanced Virgo has joined the two LIGO detectors
76 for the 2nd observing run (O2), improving the accuracy in the determination of the origin of the
77 signals and assuring that candidates are valid gravitational wave-events [3].

78 Like several facilities hosting scientific apparatus similar to Virgo [4-6], high-precision geodetic
79 surveying activities are usually carried out also for monitoring the stability of the infrastructure and
80 supporting the realignment procedures after maintenance works or during implementation stages.

81 This paper describes the surveying activities performed at the Virgo site, concerning both the
82 VRS establishment and the analysis of the monitoring data. The first section contains a summary of
83 the surveying methodologies and the processing strategy adopted to perform the network
84 adjustment that provided the final set of coordinates of the VRS network. The second section reports
85 the monitoring activities conducted over the years, mainly consisting of regular high accuracy
86 levelling surveys, periodically integrated by GPS and robotic Total Station measurements. In order
87 to improve the knowledge on the long-term trend of the settlements affecting the Virgo
88 infrastructures, an analysis based on differential interferometry using satellite Synthetic Aperture
89 Radar (SAR) data has been performed and compared with the outcome from in-situ data.

90 2. Establishment of the Virgo Reference System

91 During the construction, surveying activities were carried out in order to implement and
92 strengthen the wide-scale high precision reference network to define the VRS. The availability of a
93 high precision reference system is fundamental to carry out all the surveying activities, needed in a
94 research facility that hosts large experimental apparatus such as Virgo [7-10].

95 More specifically, the geodetic activities concerning the VRS are focused on:

- 96 • Alignment of the new equipment installed for AdV and displacement of the existing ones;
- 97 • Determination of the position of the internal components of the detector (mirrors, payloads,
98 super-attenuators, in-air benches, suspended benches, etc.) in the VRS as the unique reference
99 system;
- 100 • Execution of periodic checks;
- 101 • Monitoring over time of the (relative) position for the several buildings hosting the scientific
102 apparatus.

103 The VRS was established by of a number of new reference points, which integrated and enlarged
104 the previous local networks, located in the buildings and in the tunnels. Considering the weakness
105 of the network geometry due to the facility elongated shape, the survey activity was conducted
106 integrating Total Station with GNSS measurements to introduce constraints between the two Virgo
107 tunnels and increase the reliability of the final VRS coordinates [11]. Additional connections between
108 the main control network and the secondary ones, placed inside the 4 experimental buildings (Central
109 Building, Mode Cleaner, West End Building and North End Building), were introduced in order to
110 obtain in all sections of the Virgo facility a set of congruent coordinates.

111 2.1 Definition of the Virgo Reference System

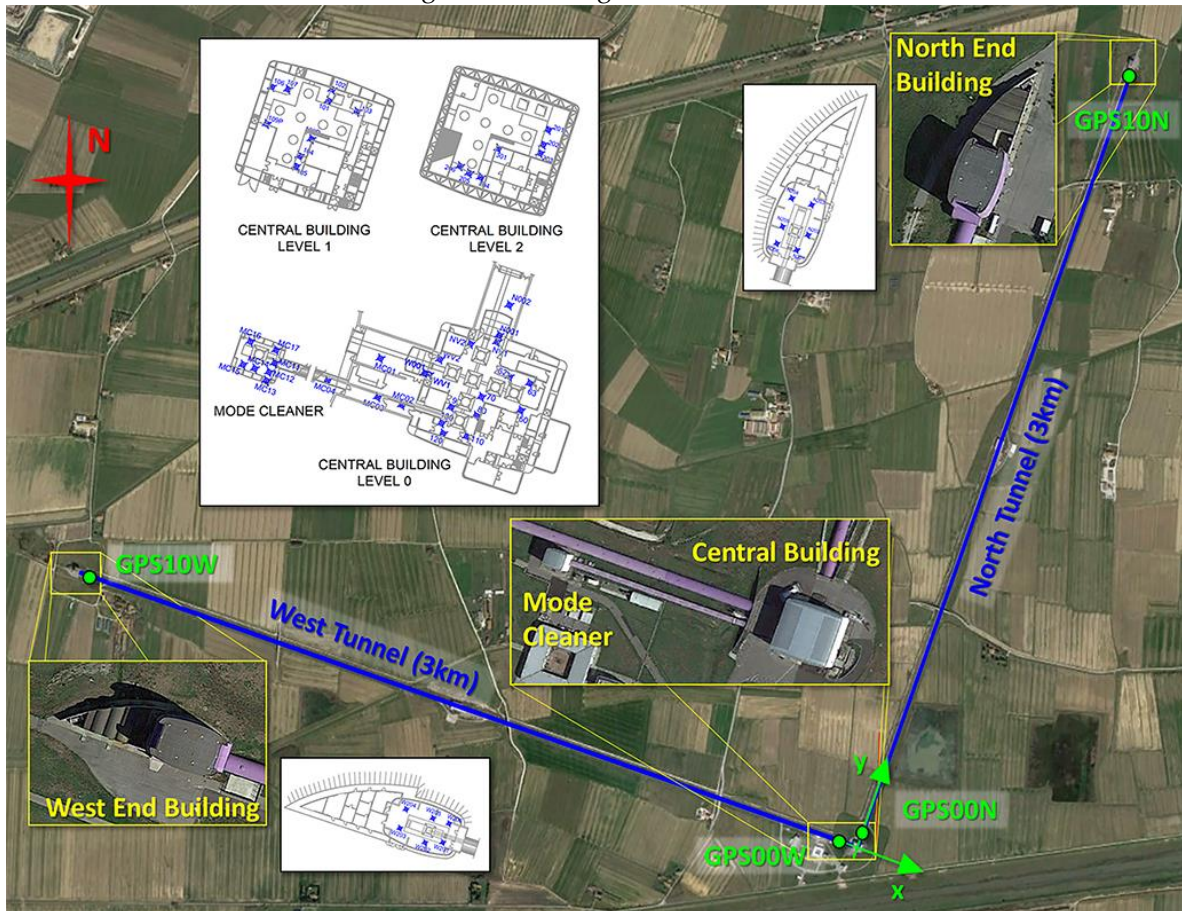
112 In the design stage of VRS a preliminary reference system was established: the two orthogonal
113 3km long arms defined a plane (Figure 1) tangent to the local sphere respect which the height was
114 computed along the two directions, while, for the horizontal component, the angle between the North
115 arm and the North UTM directions was defined.

116 A first geodetic reference frame (in the following called oldVRS) realized by ground based
117 measurements was adopted to carry out the first alignments until 2003 and adopted to perform
118 periodic resettlement of different part of the infrastructure. At the time of VRS realization only a few
119 reference points were still accessible.

120 The current Virgo Reference System is defined by fixing the alignment along two GNSS points
121 (GPS00N-GPS10N) established along the North Arm. The direction of the y-axis is quasi- parallel to

122 the North Arm and the x-axis accordingly perpendicular to the y-axis (Figure 2). The origin of VRS
123 has been kept unchanged respect to the oldVRS. The z-axis is oriented respect to the local sphere.

124 As shown in Figure 2, the VRS frame is composed by four local high precision secondary
125 networks (characterized by distances below 25 meters) located inside the experimental buildings at
126 the centre and the end of two orthogonal 3 km long arms.



127
128 **Figure 2.** Complete layout of the Virgo facilities and main VRS internal reference points (blue points),
129 located inside the four experimental buildings. Green points show the position of the four GNSS
130 stations used to integrate the total station survey.

131 The VRS network includes 11 points located along each tunnel: GPS00N... GPS10N, GPS00W...
132 GPS10W using a device designed by EGO during previous GPS surveys to guarantee a precise
133 antenna positioning for the monitoring of the vertical/horizontal displacements of the tunnels. Two
134 of them (GPS00N and GPS10N) were used to define the reference system. Moreover, 4 external
135 concrete pillars (C6-C9 in Figure 3) close to the CB allow the connection between inside and outside
136 network. Finally, levelling benchmarks were established since 2001 for the soil settlement monitoring
137 as described in the next sections. The following table (Table 1) resumes the number and location of
138 the network points including those established in the period 2012-2014 to define the VRS.

139
140 In consideration of the dimension of the network and the necessity to link the external network
141 with the internal one, it was decided to integrate Total Station (TS) measurements with GNSS
142 baselines. This integrated approach not only increased the robustness of the network but also allowed
143 to established links between the terminal parts of the two tunnels, not mutually measurable with
144 optical instruments. Due to the high accuracy required for the Virgo equipment positioning, the
145 measurements were planned and realized to estimate the points coordinates with a precision of few
146 millimetres.

147

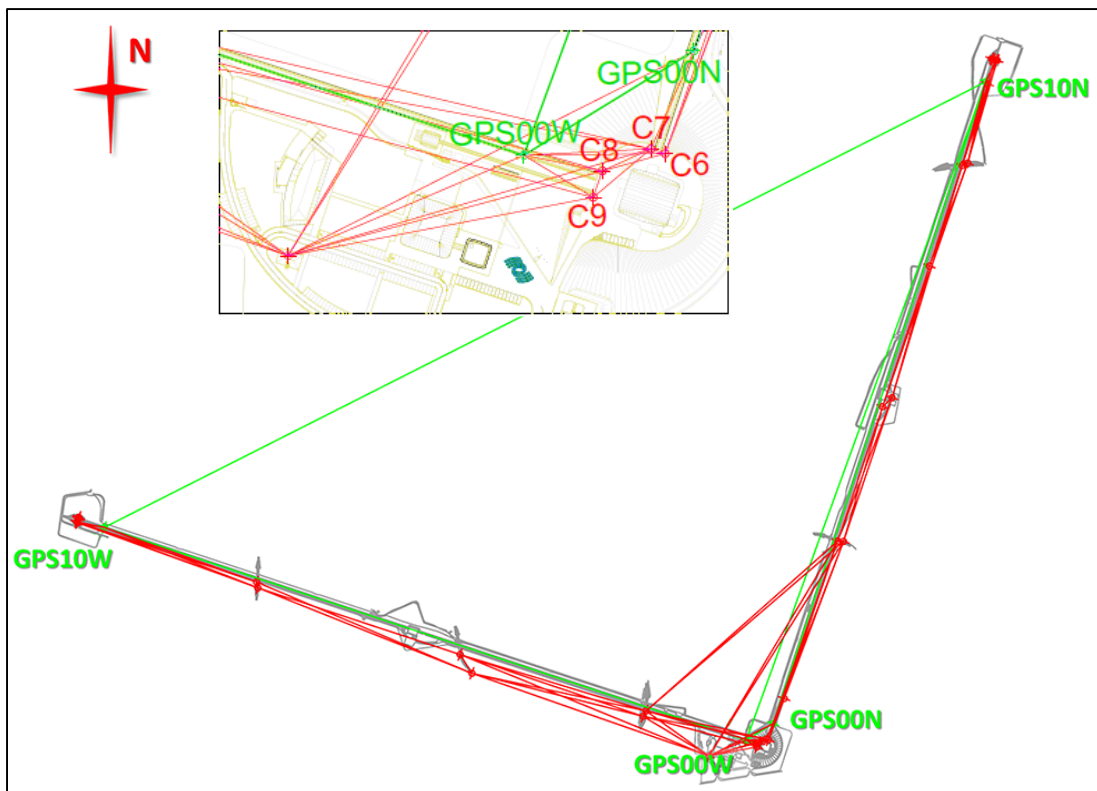
Table 1. Number and location of the network points.

Location		Number of Points		
		TS	GNSS	Levelling
Central Building	Level 0	19	---	8
	Level 1	9	---	---
	Level 2	7	---	---
Mode Cleaner Building		14	---	14
West End Building		6	---	6
North End Building		6	---	6
North Arm		209	11	209
West Arm		209	11	209
Outside (pillars)		34	12	30

149

150 ~~In consideration of the dimension of the network and the necessity to link the external network~~
 151 ~~with the internal one, it was decided to integrate Total Station (TS) measurements with GNSS~~
 152 ~~baselines. This integrated approach not only increased the robustness of the network but also allowed~~
 153 ~~to established links between the terminal parts of the two tunnels, not mutually measurable with~~
 154 ~~optical instruments. Due to the high accuracy required for the Virgo equipment positioning, the~~
 155 ~~measurements were planned and realized to estimate the points coordinates with a precision of few~~
 156 ~~millimetres.~~

157 The TS measurements were performed starting from the 4 concrete pillars, located in the external
 158 area close to the Central Building, previously connected with the network inside the building.
 159 Additional points were positioned along the arms and on the bridges passing over the tunnels. This
 160 allowed to perform optical measurements linking the Central Building with the North and West End
 161 Buildings. The final VRS network configuration is reported in Figure 3.
 162



163 **Figure 3.** Complete layout of the VRS surveyed network: green lines show the GNSS network and red lines
 164 the external TS network, distributed along the arms.

165 **2.2 Network measurement**

166 The four local networks were measured in three different TS campaigns carried out between
 167 2012 and 2013 using two high precision total stations (Leica TS30 and the TCA2003). Considering the
 168 limited size of the network connections, a special attention was given to method adopted for station
 169 centring: on the reference pillars the instrument was mounted on a calibrated plate while in case of
 170 tribrach mounting a nadir optical plummet Wild NL, characterized by an accuracy of ± 0.5 mm at 100
 171 m, was used. Besides, all stations were previously aligned along the vertical by the TS dual axis
 172 compensators (setting accuracy 0.5").

173 The surveying to connect the local networks was carried out during four campaigns in 2014
 174 using a long-range Leica TM50 and a Leica TDA5000, both motorized instruments, characterized by
 175 high precision standards, $\sigma_{\alpha}=\pm 0.5''$ on the angular observations and $\sigma_d=\pm(0.6\text{mm}+1\text{ppm})$ and
 176 $\sigma_d=\pm(1\text{mm}+2\text{ppm})$ on the distance, respectively. The TM50 was used for the long-distance
 177 measurement. The first two campaigns allowed to connect the 4 external pillars to the external part
 178 of the North and West End Buildings; the third and the fourth ones allowed to connect the external
 179 surveys with the reference points located in the experimental buildings.

180 The observations of slope distance, azimuthal and vertical angle were repeated three times in
 181 both the telescope positions (face left and face right), using the Leica Automatic Target Recognition
 182 (ATR) technology in order to achieve more consistent results.

183 The GNSS survey was performed in 2014 (JD 192÷194) using five geodetic receivers (four
 184 Trimble 5700 and one Topcon GB100), all of them connected to Choke Ring antennas. The acquisitions
 185 were composed by 24 hours lasting sessions (Figure 4). Each session was processed separately using
 186 the Bernese GNSS scientific software v.5.0 [12] to obtain a network solution including 10 GNSS
 187 stations of the IGS Permanent Network linked to the ITRF08 reference frame.



188
 189 **Figure 4.** GNSS antenna mounted on the tunnel.

190 The solutions of the three sessions were adjusted, obtaining the results summarized in Table 2.

191 **Table 2.** Solution of the GNSS processing

Point ID	X (m)	Y (m)	Z (m)	σ_X (m)	σ_Y (m)	σ_Z (m)
GPS00N	4546307.124	843013.321	4378645.366	0.001	0.001	0.001
GPS10N	4544331.414	843601.216	4380569.835	0.001	0.001	0.001
GPS00W	4546373.099	842910.486	4378597.265	0.001	0.001	0.001
GPS10W	4546219.966	840177.392	4379274.960	0.001	0.001	0.001

192

193 2.3 Data reduction into the VRS

194 The final coordinates of the network were obtained adopting a rigorous method for the least
195 squares adjustment. A procedure to make all the observation homogeneous in term of reference
196 systems was applied before conducting the network adjustment and then the roto-translation into
197 VRS (Figure 5).

198 In particular, the TS observations (angles and distances), referred to Local Reference Frame
199 (LRF) and the GNSS baselines, referred instead to a geocentric Cartesian system, were brought to a
200 common Eulerian Reference System (ERS) established with the origin in the Central Building,
201 choosing xy plane tangent to the local sphere with the y axis along the North direction.

202 Therefore, the GNSS coordinates were transformed from the adopted Cartesian geocentric
203 reference system (ITRF08) to the defined ERS by the analytical transformation:

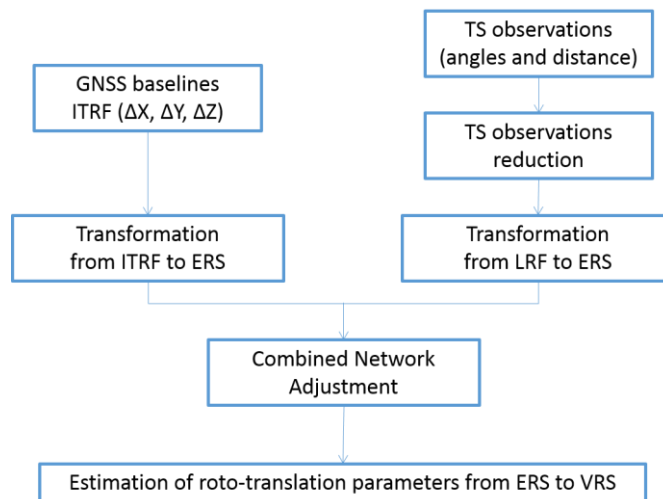
204
$$\mathbf{X}_{ERS} = R(\varphi_0, \lambda_0)(\mathbf{X} - \mathbf{X}_0) \tag{1}$$

205 setting the approximate ERS origin inside the central building (Table 3).

206 **Table 3.** Coordinates of the ERS origin

	φ_0	λ_0	H_0 (m)	X_0 (m)	Y_0 (m)	Z_0 (m)
Origin	10° 30' 16''	43° 37' 53''	9.0	4546337.287	842981.326	4378541.338

207

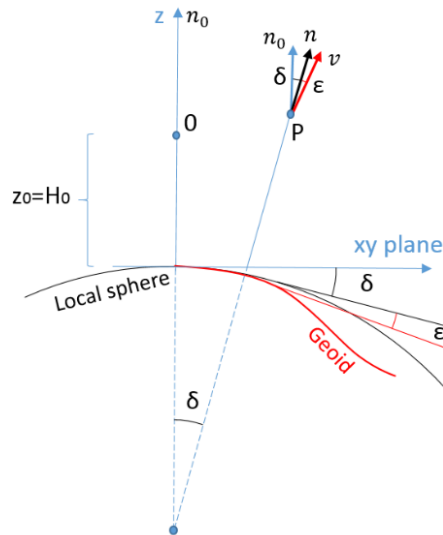


208

209 **Figure 5.** Scheme of GNSS and TS measurements integration and their alignment to VRS

210 The TS measurements were corrected according to the approach proposed by [13]. Due the
211 network extension, it was necessary to consider the terrestrial curvature: the network adjustment was
212 performed combining a spherical reference surface with a 3D Cartesian coordinate system, as shown
213 in Figure 6.

214



215

216

217

Figure 6. ERS and geodetic reference surface approximation: combined effects of vertical deflection (ϵ) and terrestrial curvature (δ).

218

219

220

221

222

223

224

225

226

227

228

229

230

231

232

233

234

235

236

237

238

In a generic point P , the direction of the vertical is rotated respect to the origin 0 of the ERS by the terrestrial curvature and by the variation of the vertical deflection. The least squares adjustment is possible by using the simple 3D Cartesian equation model, applying to the observations a set of correction factors. The correction for the terrestrial curvature was easily calculated by approximated coordinates: angle observations needed corrections ranging from 55^{cc} to 300^{cc} , considerably minor in the horizontal angles rather than on the vertical ones. Meanwhile, as stated in [13], the variation of the deviation of the vertical was neglected thanks to the short distances involved ($<10\text{km}$).

The least square network adjustment, performed with the scientific software CALGE [14], provided the best estimate of the coordinates including their precision.

The software requires as input a redundant number of observations to form the equations for each 3D ranges, azimuthal, zenithal angles and the ERS baseline components. Error models for GNSS baselines and accuracy defined according to the TS specifications were also adopted.

A preliminary computation has been performed using only the TS angular measurements in order to identify outliers before the final network adjustment that includes also GNSS baselines, as described in Figure 3 (green connections) in order to improve the geometry.

Considering that the distances between the surveyed points range between 5 m and 1500 m, the error model (weights) for the TS observations was defined as a function of the distance, in order to balance the effects of the collimation error for different distances. A sensitivity analysis to refine the overall error model was performed, providing the results reported in Table 4 and 5, for distance and angles respectively. The final adjustment provided results with standard deviation lower than 1 mm for the xy coordinates and lower than 1.5 mm for the z .

239

Table 4. A priori standard deviation for distance observations used in the network adjustment

Distance (m)	TM50		TDA5000	
	Fixed error (mm)	Proportional Error (ppm)	Fixed error (mm)	Proportional Error (ppm)
$<200\text{m}$	0.6	1	1	2
$\geq 200\text{m}$	1	1	1.5	2

240

241

Table 5. A priori standard deviation of angle observations used in the network adjustment

Distance (m)	TM50	TDA5000
--------------	------	---------

	Horizontal angle (grad)	Vertical angle (grad)	Horizontal angle (grad)	Vertical angle (grad)
<5	$2 \cdot 10^{-3}$	$3 \cdot 10^{-3}$	$2 \cdot 10^{-3}$	$3 \cdot 10^{-3}$
5-10	$1.5 \cdot 10^{-3}$	$2.5 \cdot 10^{-3}$	$1.5 \cdot 10^{-3}$	$2.5 \cdot 10^{-3}$
10-50	10^{-3}	$2 \cdot 10^{-3}$	10^{-3}	$2 \cdot 10^{-3}$
50-200	$0.8 \cdot 10^{-3}$	$1.5 \cdot 10^{-3}$	$0.8 \cdot 10^{-3}$	$1.5 \cdot 10^{-3}$
>200	$0.5 \cdot 10^{-3}$	10^{-3}	$0.5 \cdot 10^{-3}$	10^{-3}

242

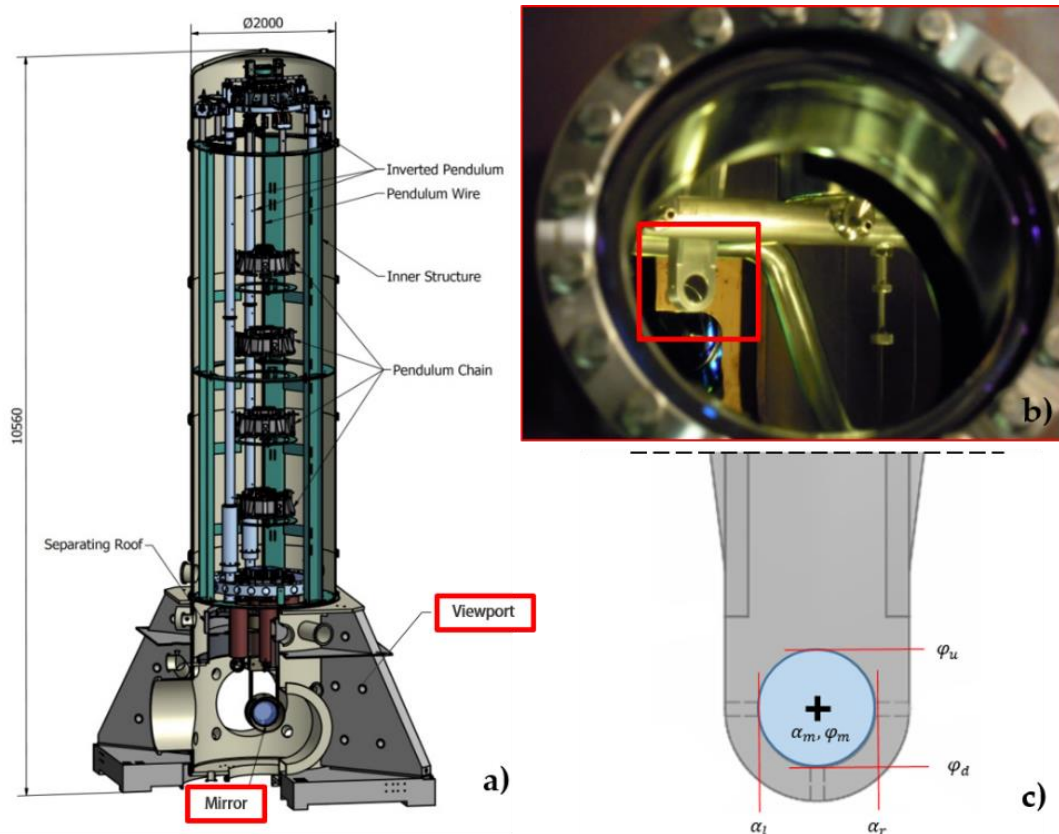
243 In order to express the network into the VRS reference system, the estimated ERS coordinates
 244 were clockwise rotated using the GPS00N-GPS10N baseline and translated to fix the origin by
 245 determining the shift parameters thanks to five points known also in the oldVRS.

246 **3. Georeferencing Virgo interferometer**

247 The establishment of the VRS reference frame and the determination of the transformation
 248 parameters between ITRF and VRS have also allowed the inverse transformation $VRS \rightarrow ITRF$ and
 249 the estimation of the ITRF coordinates of the Virgo Control Points (VCPs).

250 VCPs are the centres of the Beam Splitter (BS), North End (NE) and West End (WE) suspended
 251 mirrors: points fully defining the location and orientation of the Virgo interferometer respect to the
 252 other Gravitational Waves detectors (LIGO Hanford, WA, USA; LIGO Livingston, LA, USA; GEO,
 253 Germany; KAGRA, Japan), contemporary observing the Universe signals.

254 Mirrors are not accessible with a direct survey because they are located inside the vacuum
 255 enclosures at the ends of the interferometer arms (Figure 7). They are visible only across two
 256 viewports at the bottom of the pendulum towers, so the centre of each mirror was indirectly surveyed
 257 by TS, collimating the edges of the metallic mirror frame across the viewport glasses. Executing the
 258 survey from both the viewports, the space resection of the VCPs was realized only by means of TS
 259 angle observations.
 260



261

262
263
264

Figure 7. Suspended mirror of Virgo detector inside the Ultra-High Vacuum system: pendulum apparatus (a), mirror view through a viewport (b) and indirect determination of the mirror centre by external mirror edges collimation (c).

265
266
267
268

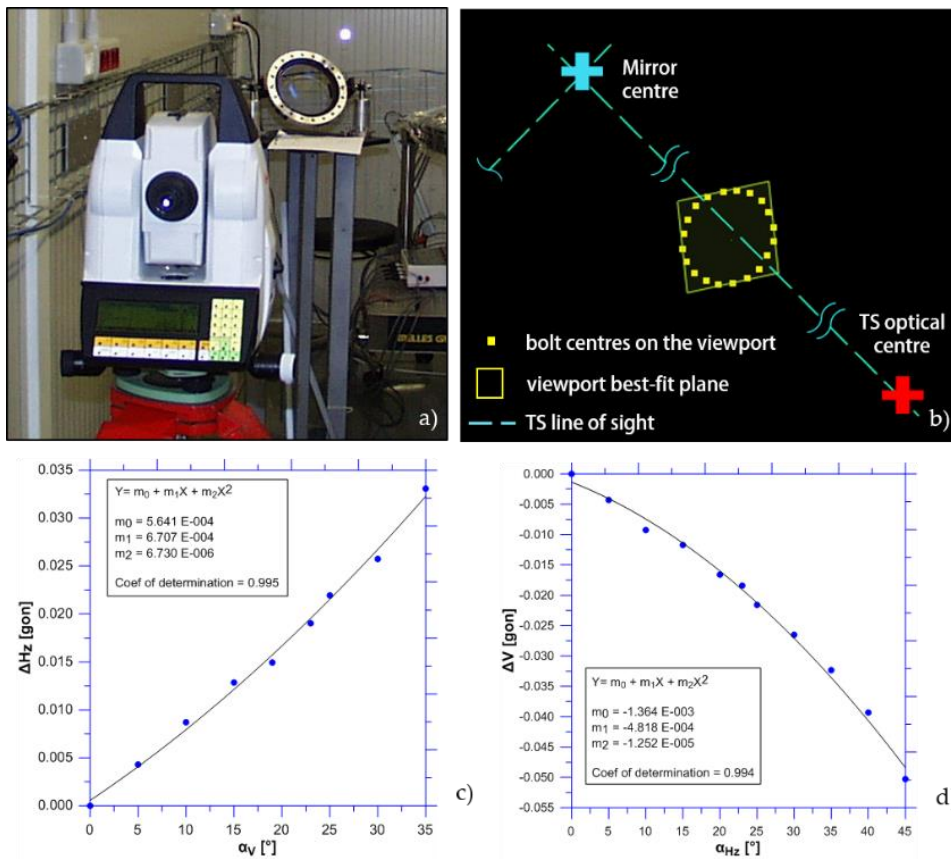
The effect of the glass optical refraction was investigated by means of angular measurements across a viewport with analogous optical and geometrical characteristics (figure 8): it was reconstructed the analytical model of the optical ray deviations, changing systematically the incidental angle of the TS line of sight.

269
270
271
272
273

The TS and mirror centres coordinates permit to define the line of sight directions. The glass plane attitude was reconstructed by means of a best-fit computation of the bolts centres, which fix the metallic frame of the viewports. The angular correction values corresponding to the estimates of the incident angles were applied to the TS observations in order to obtain a reliable set of coordinates for the mirrors centres.

274
275
276
277
278

The VRS coordinates of VCPs transformed into ITRF08 allowed also to determine the global alignment of the local network with respect to the North. The azimuth of the geodesic curve through BS and NE, with respect to the North, is $19^{\circ} 25' 58''.7265$. The azimuth of the geodesic curve through BS and WE, with respect to the North, is $289^{\circ} 25' 58''.5720$.



279

280
281
282
283

Figure 8. Experimental investigation about the effects of glass viewport crossing on angular observations: repetitions of TS measurements with different incident angles in laboratory (a), reconstruction of the incidental angle between the TS lines of sight and the glass plane during survey (b), analytical models of the ray deviations (c, d).

284

4. Soil settlement monitoring

285
286
287
288

The existence of a subsidence phenomenon in the area of the Virgo interferometer was well known since the early designing phase of the civil engineering works [15, 16]. Therefore, all the relevant infrastructures were designed considering this effect based on several geotechnical studies carried out considering the characteristics of the soil present in the area. Intensive geological surveys

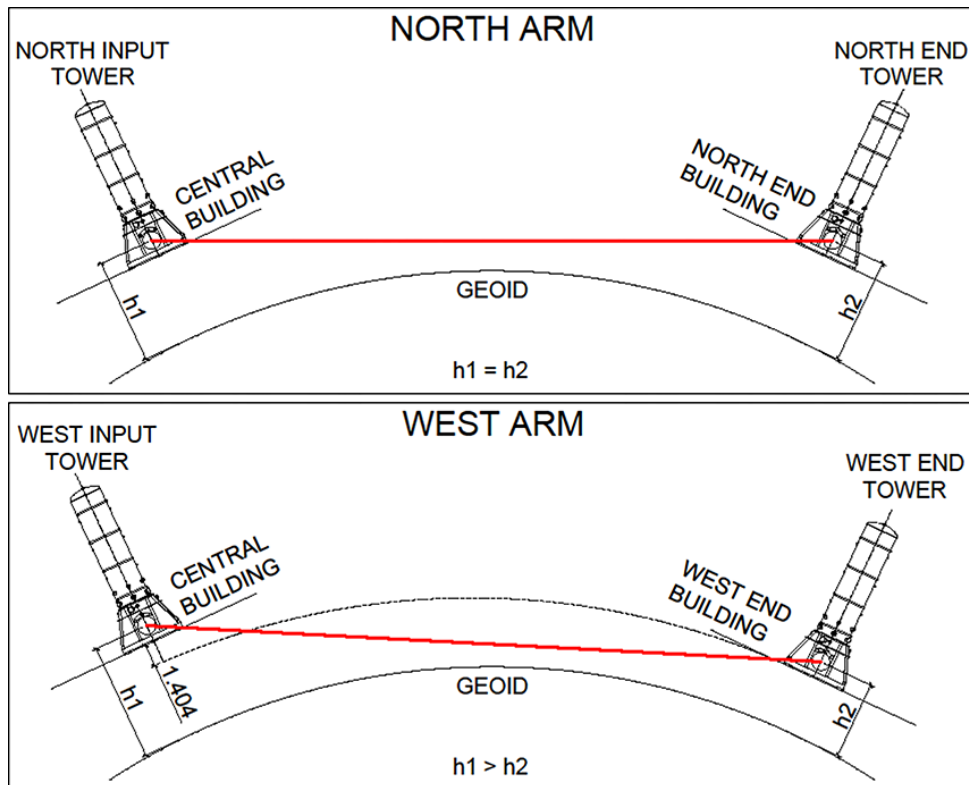
289 [17, 18] were performed in order properly define the soil characteristics and to model the expected
290 settlement pattern in response to the loads. Nevertheless, the need to monitor the displacements and
291 compare these with the expected values, as well the tight specifications set for hosting the Virgo
292 interferometer, have required a continuous surveying activity to control the position of the buildings.

293 The main monitoring activity at Virgo site is devoted to control the subsidence processes
294 activated in the area due to the overload of the constructions considering that there are two
295 fundamental conditions to be fulfilled:

- 296 • For optical requirements, the interferometer has to lay in a 3x3km plane (vertical displacement
297 less than 5 mm per month, less than 10 mm per year; less than 150 mm in 20 years) and the
298 tunnel axes have to be orthogonal with an accuracy of ± 0.02 mrad;
- 299 • The operation along the two 3km-long UHV tubes requires that relative settlement of any pipe
300 cross section is kept less than 5 mm compared to the previous survey, as limit of stress for the
301 vacuum tube welding.

302 At the design stage in 2001, in order to accomplish the morphology of the area, the topographic
303 height of the beam (suspended mirror centre) was set the same at Central and North End Buildings,
304 while a difference of -1.404 m was established between the Centrale and the West End Building
305 (Figure 9).

306



307

308 **Figure 9.** Schematic profiles of the two orthogonal 3km long arms forming the Virgo laser
309 interferometer, showing the initial offset of the End Buildings with respect the Central Building at the
310 start of the monitoring.

311 The monitoring consists of topographic measurements to check the differential displacements
312 between two adjacent modules (distance 15 m). In addition to the direct measurements, an
313 application of Differential Interferometry using Synthetic Aperture Radar (DInSAR) was performed
314 as described in the following paragraph.

315 Defining an accurate VRS is the technical prerequisite for the monitoring activities concerning
316 the relative positions of the different components of the interferometer. For the evaluation of relative
317 displacements, every sets of measurements carried out over the years has been reduced in the VRS

318 relative reference system with respect to the optical centre of the interferometer, located in the Central
319 Building.

320 4.1. Topographic monitoring

321 Since 2001 over 500 internal reference points and 30 external concrete pillars of VRS network
322 were periodically measured. Realignment procedures have to be carried out when the relative
323 displacement between two modules exceeds a threshold of 5 mm, from previous survey. The
324 threshold is lowered to 2 mm for the special modules attached to the large vacuum tube valves, close
325 to the experimental buildings (Figure 10).



326

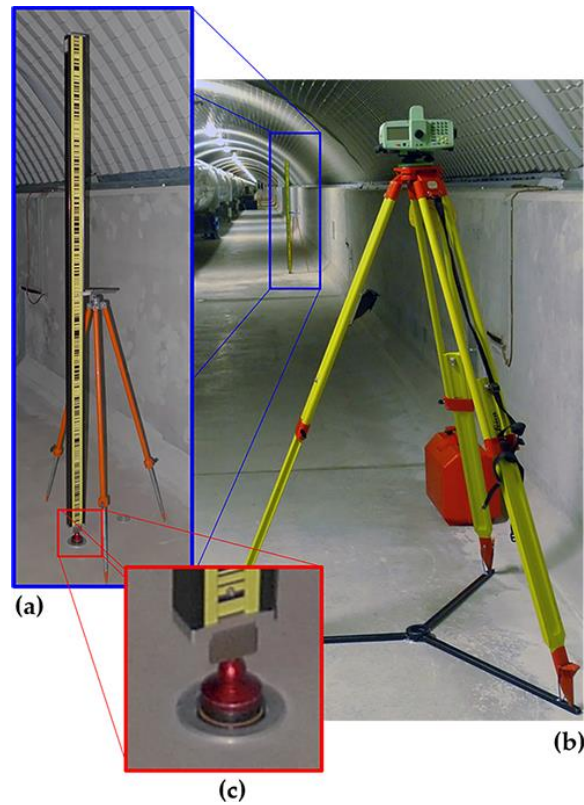
327 **Figure 10.** End Building-Tunnel link module. Special tube support with micrometric mechanical
328 realignment system.

329 The monitoring measurements along both tunnels (West and North Arms), carried out since
330 2001, include high-precision levelling and GPS surveys. Being the main purpose, the evaluation of
331 the relative displacements referred to the optical centre of the interferometer, all surveys have been
332 reduced to the zero points located in the Central Building. Also, the mutual position of these two
333 main reference points has been checked by periodic accurate levelling, in order to observe the whole
334 evolution of the interferometer.

335 Periodically, GPS measurements in combination with TS measurement to monitor horizontal
336 displacement while leveling for vertical displacement were realized to check horizontal
337 displacements. In order to maintain the expected accuracy requirements, the following conditions
338 were adopted (figure 11):

- 339 • Inter-distance of 15 m between the benchmarks along the tunnels;
- 340 • Reference points materialized by accurate centring system;
- 341 • Staff positioned with tripod on each point;
- 342 • Similar environmental conditions (temperature and relative humidity);
- 343 • Not significant air flows in the tunnels;
- 344 • Same tolerances adopted for the setup of the instruments.

345 The instruments adopted are the TS Leica TDA5000 for the initial survey, optical level Leica
346 NA2+ GPM3 for the first levelling, and digital level Leica DNA03 since 2003 to now. The frequency
347 of the measurement campaigns has been gradually decreased over the years from the initial 6 months
348 up to 24 months, in function of the soil settling.



349

350 **Figure 11.** High precision equipment adopted for the levelling along the tunnels: a) Leica DNA03
 351 station, b) rod on a reference point set by tripod and c) accurate 3D centring system of reference points
 352 placed on the tunnel floor.

353 The main levelling parameters are summarized in the following Table 6, which also reports the
 354 max e min error of closure obtained among the whole measurement campaigns.

355

Table 6. Summary of levelling parameters.

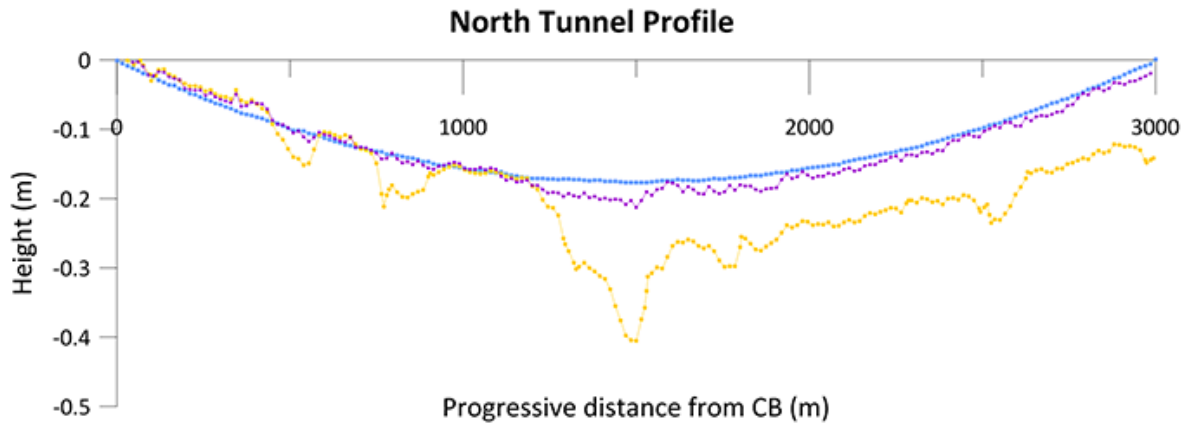
Line length	Number of stations	Max closure error	Min closure error	Max closure error	Min closure error
3006 m /line	205 /line	4.42 mm	3.76 mm	1.26 mm	0.03 mm

356

357 *4.2. Settlement data analysis and results*

358 The monitoring activity revealed since 2002 a steady subsidence process over the years because
 359 of the building and embankment overloads.

360 The following Figures 12 and 13 show trend diagrams of elevation components, where last
 361 survey of the tunnel profile is compared with the theoretical design position and the tube axis profile
 362 effectively realigned, sum of the operations since the start of the realignment process. Note that in
 363 such diagrams the x-coordinate represents the progressive distance from the Central Building as
 364 rectified geoid.
 365



366

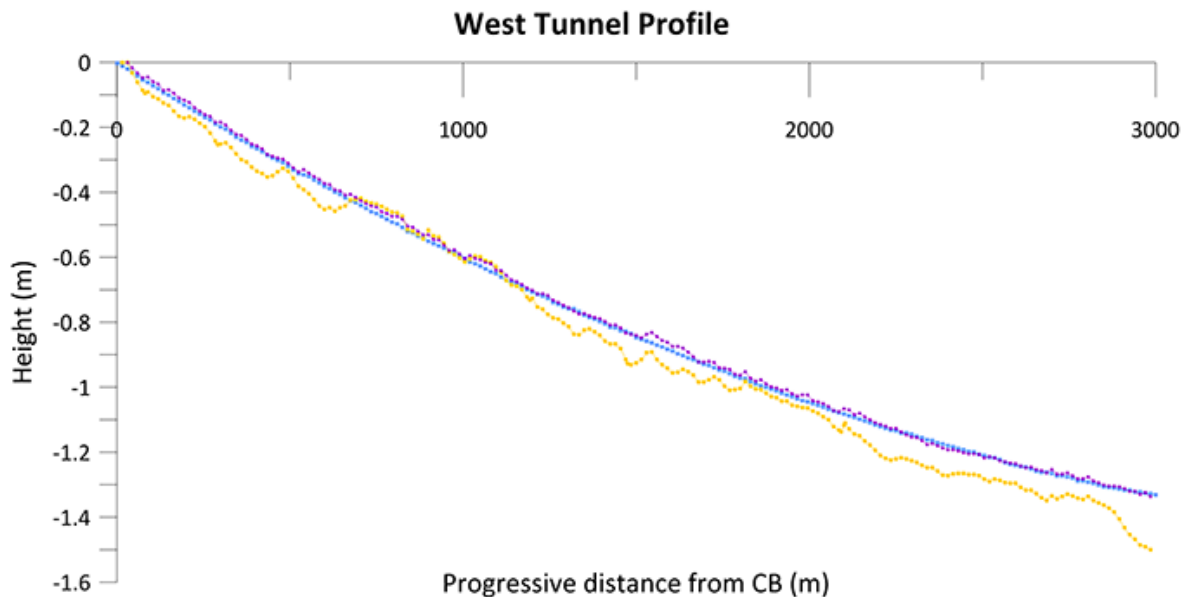
367

368

369

Figure 12. North Tunnel Profile: theoretical tracking curve (light blue); cumulated displacements at Feb 2017 (yellow); realigned profile made by the sum of the realignment activities over years 2003-2017 (purple).

370



371

372

373

374

Figure 13. West Tunnel Profile: theoretical tracking curve (light blue); cumulated displacement at Jan 2017 (yellow); realigned profile made by the sum of the realignment activities over years 2003-2017 (purple).

375

376

377

378

379

380

381

382

Analysing the data collected during the years it is possible to foresee an evolutive scenario of the phenomenon. A best-fitting curve analysis was performed on the tunnel areas showing the most pronounced effects. Particularly, these are located in the middle part of the North Tunnel (reference points N100) and in the zone of the West Tunnel next to the West End Building (reference points W199 and W200). These locations are not surprising, since those areas were interested by the major embankment overloads for the construction of the adjacent buildings. Indeed, most important settlements of the tunnels have been surveyed in correspondence of overloads on soil, related to civil works.

383

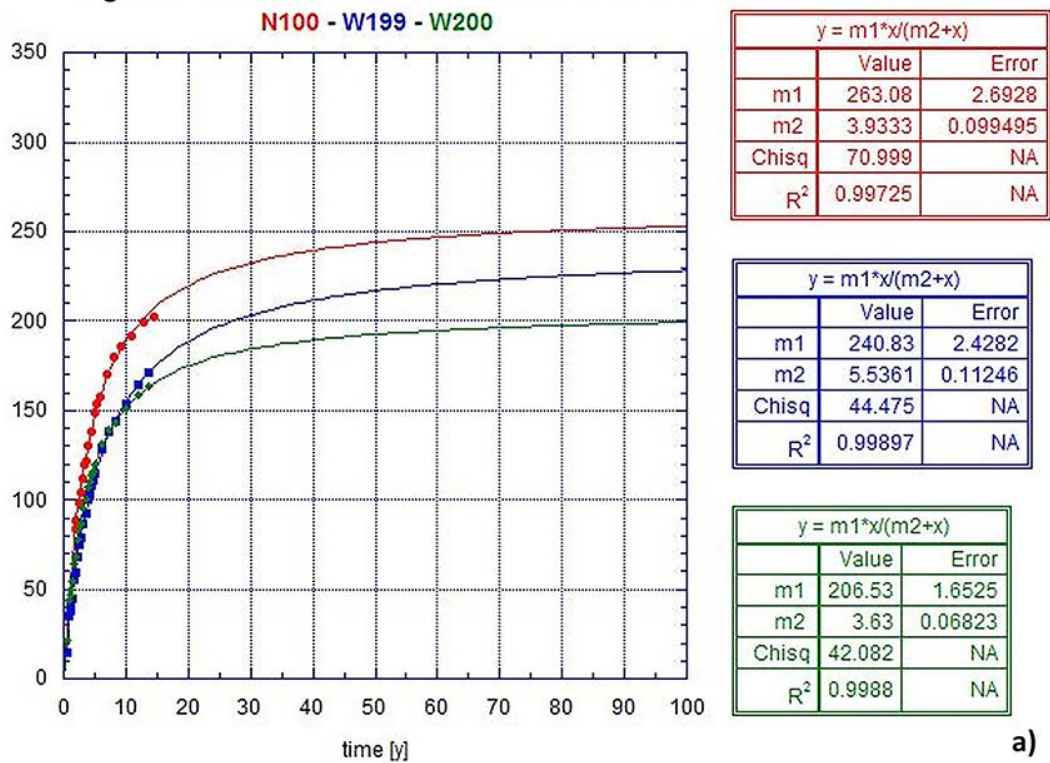
384

385

386

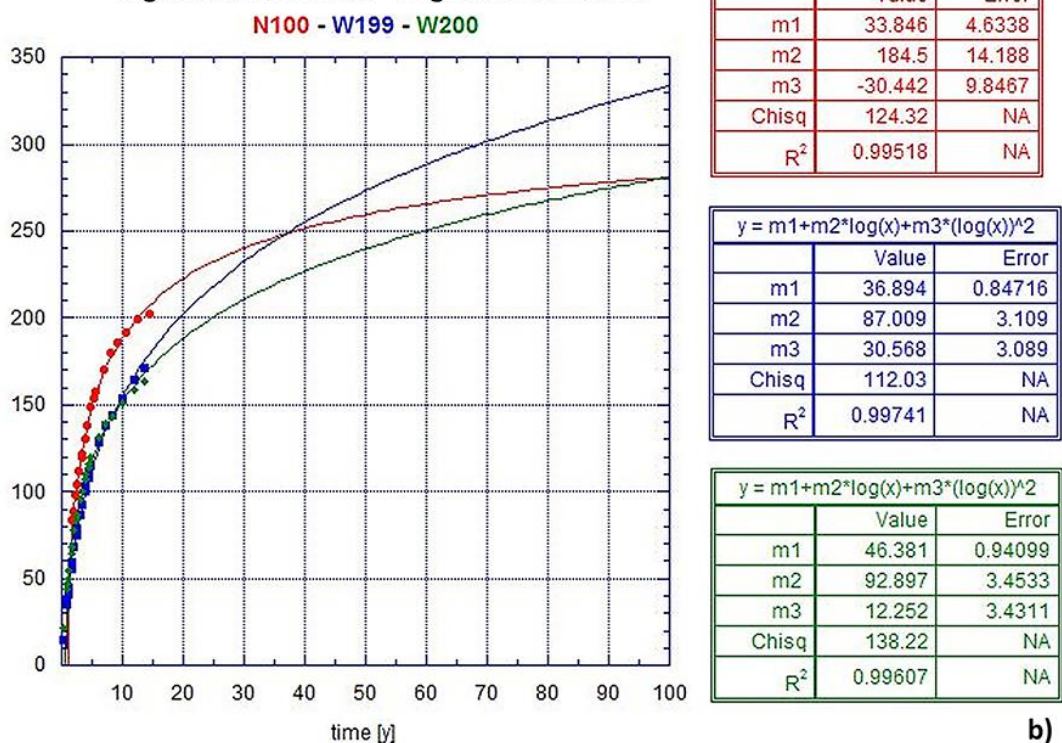
Several types of fitting curves were considered and, among them, the "Michaelis-Menton" law or the logarithmic law of order 2 provided the highest value of the coefficient of determination R^2 . The first curves are more coherent with the empirical formulas available in geotechnical literature. Figure 14 shows the diagrams for a projection over 100 years (to be considered as $t=\infty$).

Highest settlements - Michaelis-Menton curves



387

Highest settlements - Logarithmic curves



388

389

390

Figure 14. Best curve fitting for the highest settlements (N100-W199-W200). (a) “Michaelis-Menton” curves; (b) logarithmic curves (software KaleidaGraph by Synergy Software).

391

392

393

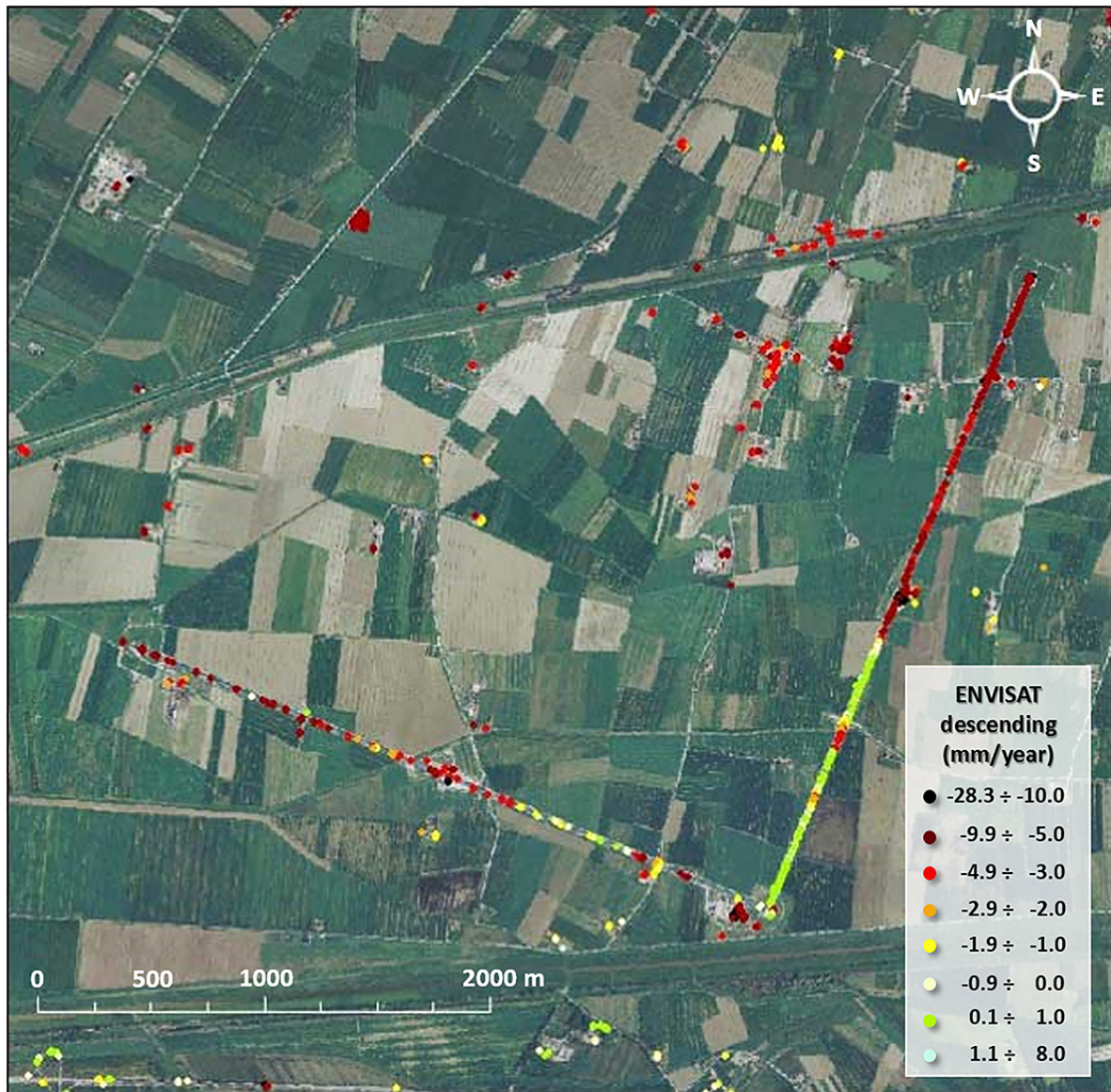
The analysis indicates that, although realignments will continue over a very long time period, the expected subsidence ($t=\infty$) is anyhow compatible with the realignment system (i.e. the length of the adjustable feet of the tube supports) and the space available inside the tunnel.

394 Clearly, these “a posteriori” hypotheses are related only to the surveyed data and focused on
395 own conditions of the Virgo tunnels and cannot be generalized. Moreover, the previous
396 considerations are based on the hypotheses that external factors will remain constant over time (i.e.
397 no large variations of the water deep stratum height in the area or new overloading of adjoining soil
398 close to the tunnels).

399 *4.3. DInSAR time series analysis and results*

400 Differential Synthetic Aperture Radar Interferometry (DInSAR) [19] is a technique based on
401 remote sensing data able to detect ground displacements. It relies on the processing of the phase
402 difference between two temporally separated SAR images. In particular, advanced DInSAR
403 approaches [20, 21] are based on the processing of SAR acquisition sequences collected over large
404 time spans to generate displacement time series of persistent scatters, that represents “targets” on the
405 surface that are able naturally to reflect radar signal (such as structures, infrastructures, etc.) without
406 the need of accessing to the site. The accuracy of DInSAR technique is estimated about centimetre to
407 millimetre [22].

408 Long-term DInSAR deformation time series have demonstrated the capability to provide
409 valuable information on the displacements that affect built up area [23, 24]. The DInSAR analysis was
410 performed to carry out an a-posteriori check on the subsidence process observed using ground-based
411 periodic surveying (levelling). Considering the level of agreement with the leveling and the capacity
412 of the DInSAR technique to measure displacement in absence of control points along the whole
413 structure and in the surrounding, it may be added to the routine monitoring schedule. This activity
414 will permit to more clearly identify the movements due to the structural overloading. Therefore, in
415 this paper was adopted this technique with the double aim: first to understand the overall settlement
416 affecting the area surrounding the Virgo interferometer and secondly to verify its performances
417 compared with classical levelling technique.
418



419

420

421

422

Figure 15. Displacement rates (mm/year) obtained applying DInSAR technique on VIRGO infrastructures and its surrounding area. The colour dots range from dark red (up to a velocity of -10mm/year) to stable points indicated in green.

423

424

425

426

DInSAR time series (acquired from Ministry of Environment and Protection of Land and Sea), obtained using a Permanent Scattering (PS) approach to process ascending and descending orbit data from ENVISAT satellite. The analysis was carried out on about 70 scenes collected on each orbit from January 2003 to June 2010.

427

428

429

430

431

432

433

434

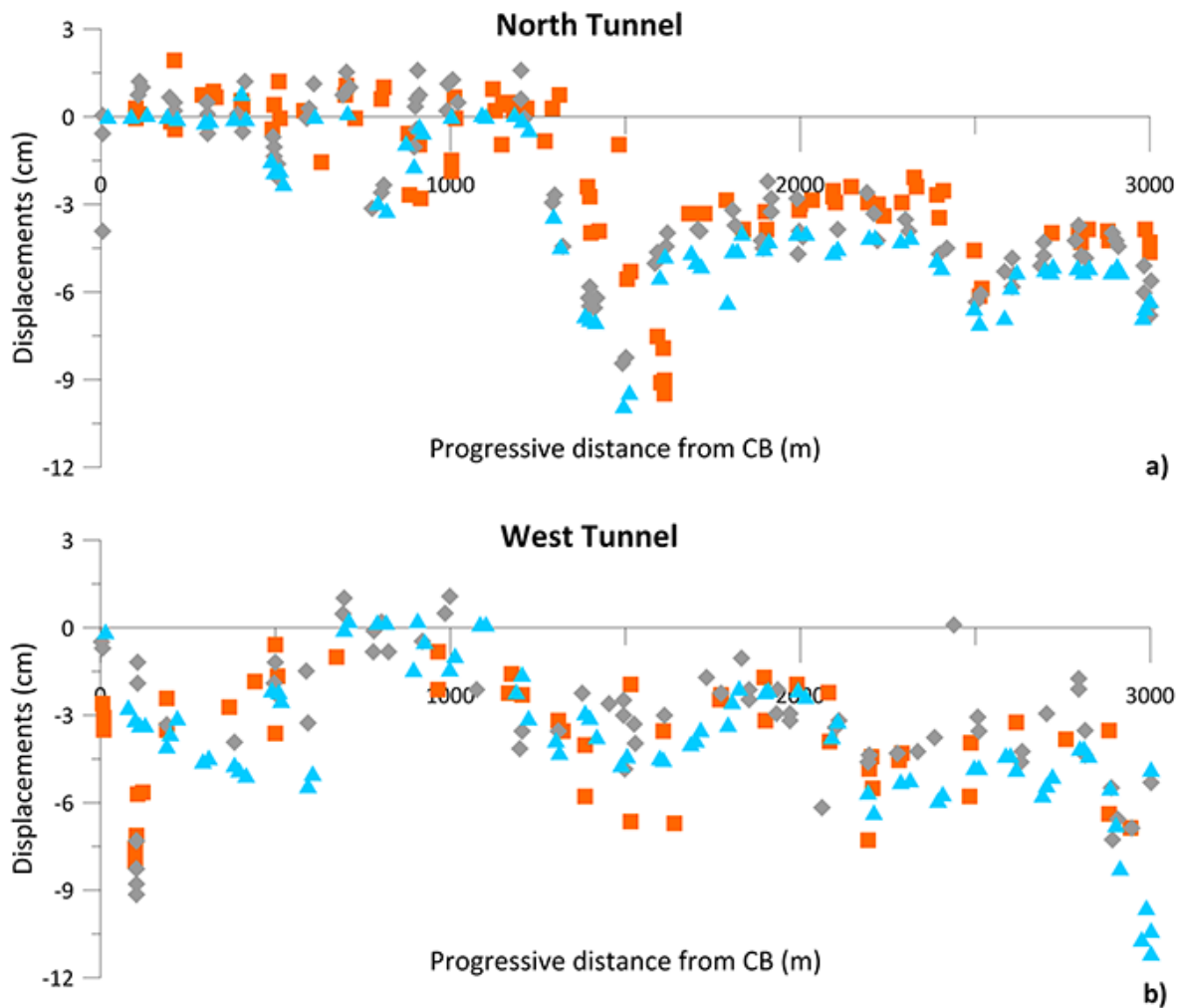
435

436

437

Figure 15 shows an overall view of the descending orbit result where colour scale dots indicates stable area (in green) and unstable area characterized by subsidence phenomena (in red). The DInSAR cumulative displacements along the North and West tunnels were compared with levelling data. Figure 16 shows the cumulated displacement of the whole 2003-2010 Envisat observation period, contemporary to the levelling sessions. These are obtained by selecting the DInSAR displacement extracted from SAR data acquired in days as much as possible close to the levelling surveying sessions. For both tunnels, the two different techniques revealed comparable subsidence trend. The displacements derived by the DInSAR data, although less accurate than the levelling ones, are characterized by larger ground coverage that allows to assess the ground subsidence phenomena at large scale. In fact, the study area is located within the Pisa alluvial plain characterized by clays and silts formations with layers of sands, peat and localized organic levels [25],

438 where the natural consolidation processes can be accelerated by overloads at the surface. DInSAR
439 data are useful to distinguish the subsidence linked to effects of the Virgo structures.
440



441
442
443 **Figure 16.** Comparison between levelling (in blue) and DInSAR data for ascending (in orange) and
444 descending (in grey) Envisat components along North Tunnel (a) and West Tunnel (b).

445 5. Conclusions

446 The construction and management of a difficult research infrastructure such as Virgo demands
447 high-precision geodetic surveying for the positioning of the instrumental parts. Besides, the extreme
448 sensitivity of the scientific facilities requires the implementation of regular monitoring to control the
449 displacements elapsing in time among the different parts of the interferometer, especially when the
450 site geotechnical setting is difficult such as at the Virgo site. Therefore, the high accuracy
451 requirements combined with the weak network geometry and the size of the connections implied the
452 integration of different techniques, based both on ground and space sensors.

453 Concerning the establishment of a local Reference System, the VRS, the integration of high
454 precision total stations and geodetic GNSS receivers offered the advantage to enforce the robustness
455 of the geodetic reference network. In particular, the use of GNSS allowed the link between the
456 terminal parts of the two tunnels of the interferometer, not mutually measurable with optical
457 instruments. Since the Virgo Control Points (VCPs) centres of the suspended mirrors were not
458 accessible, their connection to the VRS was possible only considering directions after having
459 modelled the refraction effect. This aspect suggests that future development should include further
460 systems to allow a direct measurement both to fully include them into the overall geodetic networks
461 and, eventually, to perform calibration tests.

462 A further relevant aspect has been the determination of the accurate geographic position of Virgo
463 respect to the other interferometers of the GW detector network, which is, in fact, fundamental for
464 the contemporary detection of signals coming from the Universe. The accuracy obtained for both the
465 VRS network points coordinates satisfies the initial specifications, considering the used instruments
466 and the adopted surveying methodologies.

467 Regular campaigns of high-accuracy levelling measurements integrated by GPS and theodolite
468 observations for the horizontal displacements permitted to quantify the evolution of the relevant and
469 expected subsidence process induced by the overloads of the Virgo structures acting on compressible
470 soils at foundation. In order to understand the overall settlement process, the evaluation of the
471 deformation patten of the Virgo area has been performed also through the DInSAR technique. The
472 comparison between the subsidence evaluated using DInSAR analyses and the direct measurement
473 by levelling provided a significant coherence in the evaluation of the general trend along the tunnels.
474

475 **Author Contributions:**

476

477 M.M. Surveying, data processing and analysis, paper writing.

478 C.N. Data processing and analysis, paper writing.

479 A.P. GNSS surveys, TS surveys, TS data processing and analysis, paper writing.

480 M.A.T. TS surveys, TS data processing and analysis, paper writing.

481 L.V. TS and GNSS surveys designing, TS and GNSS surveys, data analysis, paper writing.

482 A.Z. GNSS surveys, GNSS data processing and analysis, paper writing.

483

484 **Acknowledgments**

485

486 The authors thanks Ing. Alberico Sonnessa, Ing. Peppe J. V. D'Aranno and Dott. José A. Palenzuela
487 Baena for their contribution to the surveying activity. We are also grateful to Ing. Chiara Volante
488 that carried out the post-analysis of DInSAR data in comparison with the levelling one for her
489 master thesis dissertation.

490 DInSAR data were acquired from the Ministry of Environment and Protection of Land and Sea
491 (pcn.minambiente.it/mattm)

492 **Conflicts of Interest:** The authors declare no conflict of interest.

493 **References**

- 494 1. Virgo Collaboration. Advanced Virgo Technical Design Report. VIR-0128-12, EGO TDS, April 2012.
- 495 2. B. P. Abbott, et al. (LIGO Scientific Collaboration and VIRGO Collaboration). Observation of
496 Gravitational Waves from a Binary Black Hole Merger. *Phys. Rev. Lett.*, 116 (2016), 061102.
- 497 3. B. P. Abbott, et al. GW170817: Observation of Gravitational Waves from a Binary Neutron Star Inspiral.
498 *Phys. Rev. Lett.*, 119 (2017), 161101.
- 499 4. M. Masuzawa, T. Adachi, H. Iinuma, T. Kawamoto, Y. Ohsawa. SuperKEKB Main Ring Tunnel
500 Motion. in International Workshop on Accelerator Alignment 2014 (IWAA14), IHEP, Beijing, China,
501 October 2014.
- 502 5. D. Missiaen, M. Duquenne. Could the AT401 replace digital levelling and "Ecartometry" for the
503 smoothing and realignment of LHC. in International Workshop on Accelerator Alignment 2012
504 (IWAA14), Fermilab, Batavia, USA, September 2012.
- 505 6. J. Volk, V. Shiltsev, A. Chupyra, M. Kondaurov, S. Singatulin, D. Fratta, A. Meulemans, C. Potier, H.
506 Wang. Hydrostatic Level Systems at Fermilab and SURF. International Workshop on Accelerator
507 Alignment 2014 (IWAA14), Fermilab, Batavia, USA, September 2012.

- 508
509
510
511
512
513
514
515
516
517
518
519
520
521
522
523
524
525
526
527
528
529
530
531
532
533
534
535
536
537
538
539
540
541
542
543
544
545
546
547
548
549
550
7. D. Missiaen, T. Dobers, M. Jones, C. Podevin, J.P. Quesnel. The final alignment of the LHC. International Workshop on Accelerator Alignment 2008 (IWAA08), Tsukuba, Japan, February 2008.
 8. D. Missiaen, P. Dewitte, J.F. Fuchs, H. Mainaud Durand, T. Dobers, M. Jones, J.C. Status report of projects activities at CERN. International Workshop on Accelerator Alignment 2014 (IWAA14), IHEP, Beijing, China, October 2014.
 9. B. O'Sheg Oshinowo, H. Friedsam. Survey of the NOvA Near Detector at Fermilab. International Workshop on Accelerator Alignment 2010 (IWAA10), DESY Hamburg, Germany, September 2010.
 10. R. Beunard, A. Lefevre, F. Legruel. The Initial Geodetic Survey for the SPIRAL2 Process Installation. International Workshop on Accelerator Alignment 2010 (IWAA10), DESY Hamburg, Germany, September 2010.
 11. S. Matsui, H. Kimura, Survey Comparison using GNSS and ME5000 for One kilometer Range. International Workshop on Accelerator Alignment 2008 (IWAA08), Tsukuba, Japan, February 2008.
 12. R. Dach, S. Lutz, P. Walser, P. Fridez. Bernese GNSS Software Version 5.2. User Manual. Astronomical Institute, University of Bern, 2015, Bern Open Publishing <http://dx.doi.org/10.7892/boris.72297>.
 13. Brovelli M.; Sansò F., Equazioni di osservazione della topografia in coordinate cartesiane locali: scrittura, linearizzazione e analisi dei relativi ambiti di validità, Boll. Di Geod. E Sci. Affin. 3 (1989) 255–274, (in Italian).
 14. Forlani, G. Sperimentazione del nuovo programma CALGE dell'ITM. Boll. SIFET 2 (1986), (in Italian).
 15. Virgo Collaboration. Feasibility Study of the civil works of the Virgo Project EGO TDS, April 1994.
 16. Virgo Collaboration. Study of the Land subsidence of Pisa plain south the Arno river. EGO TDS, December 1994.
 17. Virgo Collaboration. First Geological Survey of the Virgo Project Area. EGO TDS, July 1991.
 18. Virgo Collaboration Second Geological Survey of the Virgo Project Area. EGO TDS, September 1994.
 19. A.K. Gabriel, R.M. Goldstein, H.A. Zebker. Mapping small elevation changes over large areas: differential interferometry, Jour. Geophy. Res., 94 (1989), 9183–9191 DOI: 10.1029/JB094iB07p09183
 20. A. Ferretti, C. Prati, F. Rocca. Non-linear subsidence rate estimation using permanent scatters in Differential SAR Interferometry, IEEE Trans. Geosci. Remote Sens., 38 (2000). DOI: 10.1109/36.868878.
 21. R. Lanari, O. Mora, M. Manunta, J.J. Mallorquí, P. Berardino, E. Sansosti. A small baseline approach for investigating deformations on full resolution differential SAR interferograms. IEEE Trans. Geosci. Remote Sens., 42 (2004), DOI: 10.1109/TGRS.2004.828196.
 22. F. Casu, M. Manzo, R. Lanari. A quantitative assessment of the SBAS algorithm performance for surface deformation retrieval from DInSAR data. Remote Sens. Environ. 102 (2006), 3-4, DOI: 10.1016/j.rse.2006.01.023.
 23. M. Bonano, M. Manunta, M. Marsella, R. Lanari. Longterm ERS/ENVISAT deformation time-series generation at full spatial resolution via the extended SBAS technique, Int. J. Remote Sens., 33 (2012), 15, DOI: 10.1080/01431161.2011.638340.
 24. S. Scifoni, M. Bonano, M. Marsella, A. Sonnessa, V. Tagliafierro, M. Manunta, R. Lanari, C. Ojha, M. Sciotti. On the joint exploitation of long-term DInSAR time series and geological information for the investigation of ground settlements in the town of Roma (Italy). Remote Sens. Environ., 182 (2016), DOI: 10.1016/j.rse.2016.04.017.
 25. G. Sarti, V. Rossi, A. Amorosi. Influence of Holocene stratigraphic architecture on ground surface settlements: A case study from the City of Pisa (Tuscany, Italy). Sediment. Geol.. 281 (2012), DOI: 10.1016/j.sedgeo.2012.08.008 .

1 Geodetic measurements to control a large research 2 infrastructure: the Virgo detector at the European 3 Gravitational Observatory

4 Maria Marsella¹, Carla Nardinocchi^{1,*}, Andrea Paoli², Maria Alessandra Tini³, Luca Vittuari³,
5 Antonio Zanutta³

6 ¹ DICEA-Survey Lab, Università di Roma "La Sapienza", Italy

7 ² EGO - European Gravitational Observatory, Pisa, Italy

8 ³ DICAM, Università di Bologna Italy

9
10 * Correspondence: carla.nardinocchi@uniroma1.it

11 Academic Editor: name

12 Received: date; Accepted: date; Published: date

14 **Abstract:**

15 The Advanced Virgo (AdV) detector is a 3 km long arms Michelson interferometer for gravitational
16 waves detection. The management of a complex and large research infrastructure requires high-
17 precision geodetic surveying for positioning and rearrangement of instruments.

18 This paper describes the establishment of Virgo Reference System (VRS) consisting in a wide-scale
19 high precision geodetic network based on GPS and Total Station measurements, that support the
20 positioning and the alignment of the different elements forming the interferometer. Ground
21 settlement monitoring is strictly required to verify and adapt the interferometer vertical alignment
22 in presence of a steady subsidence process due to infrastructures overloads. The paper describes
23 also the monitoring activity conducted over the years by means of periodic high precision levelling,
24 that was compared with the results with those obtained using differential interferometry based on
25 satellite Synthetic Aperture Radar (SAR) data

26 **Keywords:** monitoring; surveying; interferometer; DInSAR; large research infrastructure; ground
27 settlements; control network.

29 **1. Introduction**

30 The Virgo detector located at the site of the European Gravitational Observatory (EGO), in the
31 countryside near Pisa, Italy (Figure 1) [<http://www.virgo-gw.eu/>] is a Michelson laser interferometer
32 formed by two orthogonal 3 kilometres long arms. Multiple reflections between mirrors located at
33 the extremities of each arm extend the effective optical length of each arm to over 300 kilometres. In
34 order to measure distance changes smaller than 10^{-18} m, the laser beams run inside two Ultra-High
35 Vacuum (UHV) pipes hosted in the arms and the test masses (that is the mirrors reflecting the laser
36 beams) are stabilized by huge anti-seismic dampers, located inside vacuum enclosures.

37 The scientific payloads are hosted in three main experimental buildings, named Central Building
38 (CB), North End Building (NEB) and West End Building (WEB).

39 The two orthogonal arms 3 km each are constituted by two resonant cavities delimited by the of
40 relevant suspended mirrors NI-NE (North Input – North End) and WI-WE (West Input – West End).
41 Both the civil structures (perfectly isostatic Gerber beams) and the supporting system of the vacuum
42 tubes, was designed to absorb differential settlements and to carry out realignment operations.
43 Currently, the periodic monitoring campaigns and the module re-alignments are based on traditional
44 surveying. More recently, a remote differential monitoring system (Hydrostatic Levelling System,
45 HLS) is adopted to support the micrometric realignment system (Fig. 10). This system is installed at

46 the most critical points, the Link Tunnel-End Buildings N200-N201 and W200-W201, and provide
47 results that are perfectly consistent with the leveling ones. DInSAR would integrate the routine
48 measurements that should be based primarily on levelling measurements considering the very
49 stringent accuracy requirements.
50



51
Figure 1. Aerial view of Virgo Site.

52 The range of frequency of the detector (from 10 to 6,000 Hz) and its very high sensitivity are
53 designed in order to allow the detection of gravitational radiation produced by supernovae and
54 coalescence of binary systems in the Milky Way and in outer galaxies. The whole interferometer
55 attains optical perfection and is extremely well isolated from the rest of the world in order to be only
56 sensitive to the gravitational waves. To achieve the required sensitivity, involved scientists have
57 developed the most advanced techniques in the field of high power ultra-stable lasers, high
58 reflectivity mirrors and seismic isolation. Comparable efforts are required to implement a reliable
59 procedure to control along the time the position and alignment of the structures and the detector
60 components based on high precision surveying procedures. Therefore, the high accuracy for the
61 levelling is required to control the relative settlement between each couple of vacuum tube support
62 and to keep the stress induced on the welding lips of the tube modules under defined limits.
63 Moreover, for optical reason, the whole interferometer has to be kept in a plane defined by the
64 position of the Beam Splitter mirror and by all the other suspended mirrors (Test Masses).

65 The Virgo project obtained the scientific goal to meet the sensitivity requirements during the
66 years 2003÷2010 and in 2011 it has received the approval for carrying out an upgrading to further
67 enhance its sensitivity. In 2012, started the construction of Advanced Virgo (AdV) [1], upgraded
68 configuration of the interferometer. AdV was designed to improve the sensitivity by a factor 10, thus
69 allowing the observation of a volume of Universe 1000 times larger. Advanced Virgo together with
70 the other Gravitational Waves (GW) detectors running in their upgraded configuration (Advanced
71 LIGO - USA, GEO600 – Germany, KAGRA - Japan) is part of the network designed for the
72 contemporary detection of the signals coming from the Universe, which will start the era of the GW
73 Astronomy.

74 After the first detection of a gravitational wave signal with ground interferometers made by
75 Advanced LIGO in September 2015 [2], recently Advanced Virgo has joined the two LIGO detectors
76 for the 2nd observing run (O2), improving the accuracy in the determination of the origin of the
77 signals and assuring that candidates are valid gravitational wave-events [3].

78 Like several facilities hosting scientific apparatus similar to Virgo [4-6], high-precision geodetic
79 surveying activities are usually carried out also for monitoring the stability of the infrastructure and
80 supporting the realignment procedures after maintenance works or during implementation stages.

81 This paper describes the surveying activities performed at the Virgo site, concerning both the
82 VRS establishment and the analysis of the monitoring data. The first section contains a summary of
83 the surveying methodologies and the processing strategy adopted to perform the network
84 adjustment that provided the final set of coordinates of the VRS network. The second section reports
85 the monitoring activities conducted over the years, mainly consisting of regular high accuracy
86 levelling surveys, periodically integrated by GPS and robotic Total Station measurements. In order
87 to improve the knowledge on the long-term trend of the settlements affecting the Virgo
88 infrastructures, an analysis based on differential interferometry using satellite Synthetic Aperture
89 Radar (SAR) data has been performed and compared with the outcome from in-situ data.

90 2. Establishment of the Virgo Reference System

91 During the construction, surveying activities were carried out in order to implement and
92 strengthen the wide-scale high precision reference network to define the VRS. The availability of a
93 high precision reference system is fundamental to carry out all the surveying activities, needed in a
94 research facility that hosts large experimental apparatus such as Virgo [7-10].

95 More specifically, the geodetic activities concerning the VRS are focused on:

- 96 • Alignment of the new equipment installed for AdV and displacement of the existing ones;
- 97 • Determination of the position of the internal components of the detector (mirrors, payloads,
98 super-attenuators, in-air benches, suspended benches, etc.) in the VRS as the unique reference
99 system;
- 100 • Execution of periodic checks;
- 101 • Monitoring over time of the (relative) position for the several buildings hosting the scientific
102 apparatus.

103 The VRS was established by of a number of new reference points, which integrated and enlarged
104 the previous local networks, located in the buildings and in the tunnels. Considering the weakness
105 of the network geometry due to the facility elongated shape, the survey activity was conducted
106 integrating Total Station with GNSS measurements to introduce constraints between the two Virgo
107 tunnels and increase the reliability of the final VRS coordinates [11]. Additional connections between
108 the main control network and the secondary ones, placed inside the 4 experimental buildings (Central
109 Building, Mode Cleaner, West End Building and North End Building), were introduced in order to
110 obtain in all sections of the Virgo facility a set of congruent coordinates.

111 2.1 Definition of the Virgo Reference System

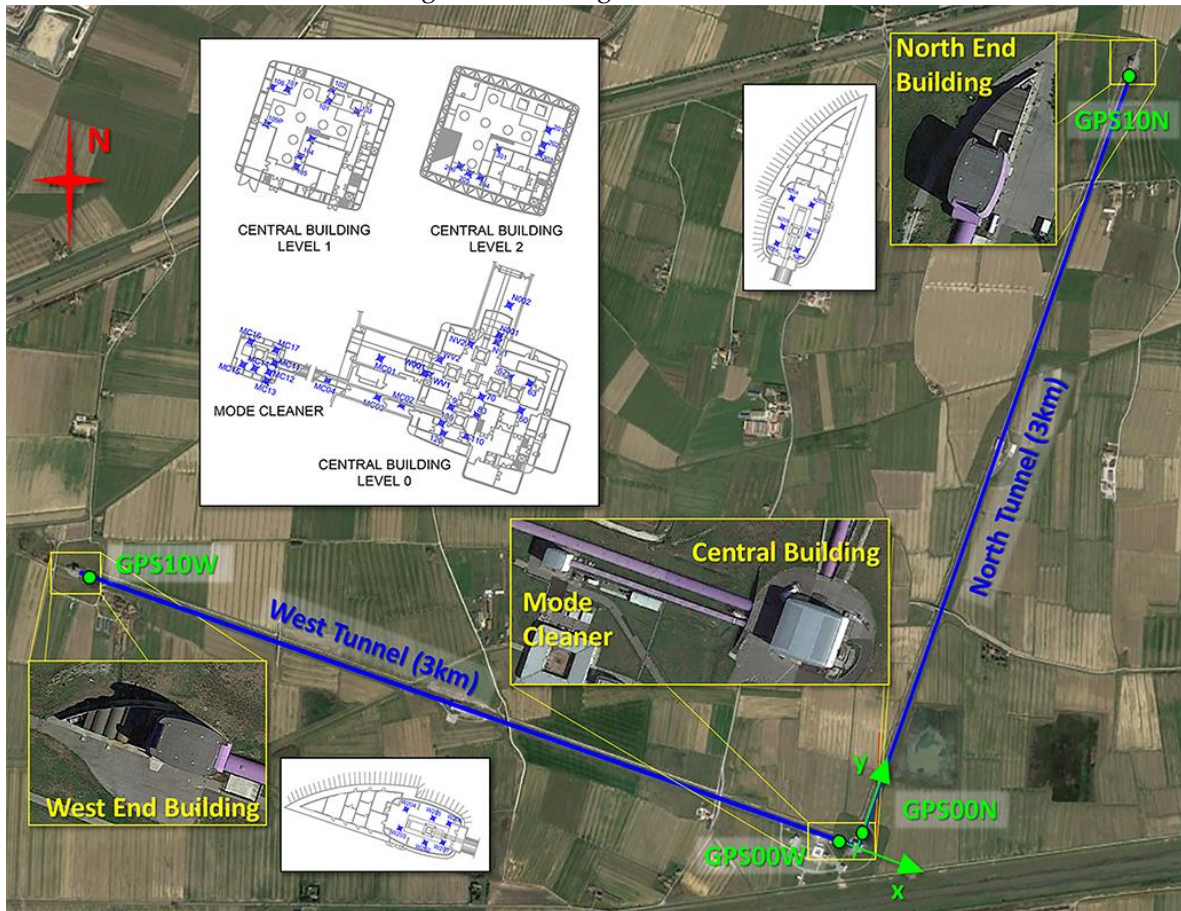
112 In the design stage of VRS a preliminary reference system was established: the two orthogonal
113 3km long arms defined a plane (Figure 1) tangent to the local sphere respect which the height was
114 computed along the two directions, while, for the horizontal component, the angle between the North
115 arm and the North UTM directions was defined.

116 A first geodetic reference frame (in the following called oldVRS) realized by ground based
117 measurements was adopted to carry out the first alignments until 2003 and adopted to perform
118 periodic resettlement of different part of the infrastructure. At the time of VRS realization only a few
119 reference points were still accessible.

120 The current Virgo Reference System is defined by fixing the alignment along two GNSS points
121 (GPS00N-GPS10N) established along the North Arm. The direction of the y-axis is quasi- parallel to

122 the North Arm and the x-axis accordingly perpendicular to the y-axis (Figure 2). The origin of VRS
123 has been kept unchanged respect to the oldVRS. The z-axis is oriented respect to the local sphere.

124 As shown in Figure 2, the VRS frame is composed by four local high precision secondary
125 networks (characterized by distances below 25 meters) located inside the experimental buildings at
126 the centre and the end of two orthogonal 3 km long arms.



127
128 **Figure 2.** Complete layout of the Virgo facilities and main VRS internal reference points (blue points),
129 located inside the four experimental buildings. Green points show the position of the four GNSS
130 stations used to integrate the total station survey.

131 The VRS network includes 11 points located along each tunnel: GPS00N... GPS10N, GPS00W...
132 GPS10W using a device designed by EGO during previous GPS surveys to guarantee a precise
133 antenna positioning for the monitoring of the vertical/horizontal displacements of the tunnels. Two
134 of them (GPS00N and GPS10N) were used to define the reference system. Moreover, 4 external
135 concrete pillars (C6-C9 in Figure 3) close to the CB allow the connection between inside and outside
136 network. Finally, levelling benchmarks were established since 2001 for the soil settlement monitoring
137 as described in the next sections. The following table (Table 1) resumes the number and location of
138 the network points including those established in the period 2012-2014 to define the VRS.

139
140 In consideration of the dimension of the network and the necessity to link the external network
141 with the internal one, it was decided to integrate Total Station (TS) measurements with GNSS
142 baselines. This integrated approach not only increased the robustness of the network but also allowed
143 to established links between the terminal parts of the two tunnels, not mutually measurable with
144 optical instruments. Due to the high accuracy required for the Virgo equipment positioning, the
145 measurements were planned and realized to estimate the points coordinates with a precision of few
146 millimetres.

147

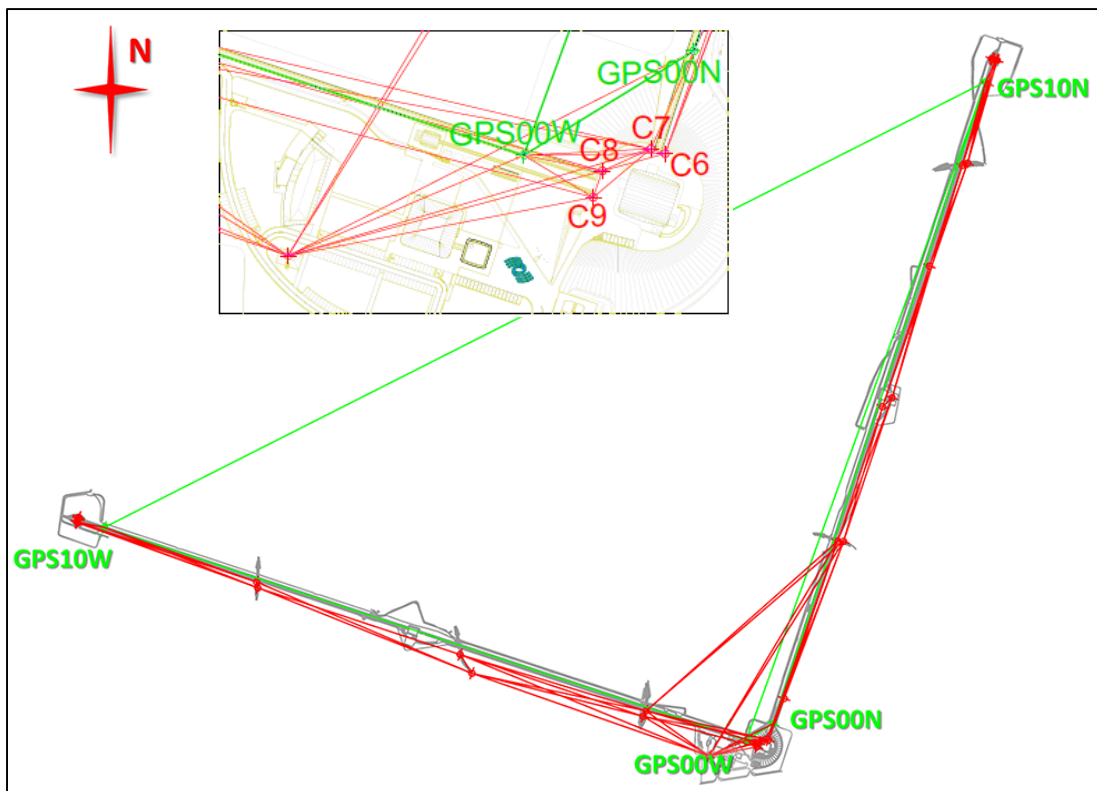
Table 1. Number and location of the network points.

Location		Number of Points		
		TS	GNSS	Levelling
Central Building	Level 0	19	---	8
	Level 1	9	---	---
	Level 2	7	---	---
Mode Cleaner Building		14	---	14
West End Building		6	---	6
North End Building		6	---	6
North Arm		209	11	209
West Arm		209	11	209
Outside (pillars)		34	12	30

149

150 ~~In consideration of the dimension of the network and the necessity to link the external network~~
 151 ~~with the internal one, it was decided to integrate Total Station (TS) measurements with GNSS~~
 152 ~~baselines. This integrated approach not only increased the robustness of the network but also allowed~~
 153 ~~to established links between the terminal parts of the two tunnels, not mutually measurable with~~
 154 ~~optical instruments. Due to the high accuracy required for the Virgo equipment positioning, the~~
 155 ~~measurements were planned and realized to estimate the points coordinates with a precision of few~~
 156 ~~millimetres.~~

157 The TS measurements were performed starting from the 4 concrete pillars, located in the external
 158 area close to the Central Building, previously connected with the network inside the building.
 159 Additional points were positioned along the arms and on the bridges passing over the tunnels. This
 160 allowed to perform optical measurements linking the Central Building with the North and West End
 161 Buildings. The final VRS network configuration is reported in Figure 3.
 162



163 *Figure 3. Complete layout of the VRS surveyed network: green lines show the GNSS network and red lines*
 164 *the external TS network, distributed along the arms.*

165 *2.2 Network measurement*

166 The four local networks were measured in three different TS campaigns carried out between
 167 2012 and 2013 using two high precision total stations (Leica TS30 and the TCA2003). Considering the
 168 limited size of the network connections, a special attention was given to method adopted for station
 169 centring: on the reference pillars the instrument was mounted on a calibrated plate while in case of
 170 tribrach mounting a nadir optical plummet Wild NL, characterized by an accuracy of ± 0.5 mm at 100
 171 m, was used. Besides, all stations were previously aligned along the vertical by the TS dual axis
 172 compensators (setting accuracy 0.5").

173 The surveying to connect the local networks was carried out during four campaigns in 2014
 174 using a long-range Leica TM50 and a Leica TDA5000, both motorized instruments, characterized by
 175 high precision standards, $\sigma_{\alpha}=\pm 0.5''$ on the angular observations and $\sigma_d=\pm(0.6\text{mm}+1\text{ppm})$ and
 176 $\sigma_d=\pm(1\text{mm}+2\text{ppm})$ on the distance, respectively. The TM50 was used for the long-distance
 177 measurement. The first two campaigns allowed to connect the 4 external pillars to the external part
 178 of the North and West End Buildings; the third and the fourth ones allowed to connect the external
 179 surveys with the reference points located in the experimental buildings.

180 The observations of slope distance, azimuthal and vertical angle were repeated three times in
 181 both the telescope positions (face left and face right), using the Leica Automatic Target Recognition
 182 (ATR) technology in order to achieve more consistent results.

183 The GNSS survey was performed in 2014 (JD 192÷194) using five geodetic receivers (four
 184 Trimble 5700 and one Topcon GB100), all of them connected to Choke Ring antennas. The acquisitions
 185 were composed by 24 hours lasting sessions (Figure 4). Each session was processed separately using
 186 the Bernese GNSS scientific software v.5.0 [12] to obtain a network solution including 10 GNSS
 187 stations of the IGS Permanent Network linked to the ITRF08 reference frame.



188
 189 **Figure 4.** GNSS antenna mounted on the tunnel.

190 The solutions of the three sessions were adjusted, obtaining the results summarized in Table 2.

191 **Table 2.** Solution of the GNSS processing

Point ID	X (m)	Y (m)	Z (m)	σ_X (m)	σ_Y (m)	σ_Z (m)
GPS00N	4546307.124	843013.321	4378645.366	0.001	0.001	0.001
GPS10N	4544331.414	843601.216	4380569.835	0.001	0.001	0.001
GPS00W	4546373.099	842910.486	4378597.265	0.001	0.001	0.001
GPS10W	4546219.966	840177.392	4379274.960	0.001	0.001	0.001

192

193 2.3 Data reduction into the VRS

194 The final coordinates of the network were obtained adopting a rigorous method for the least
195 squares adjustment. A procedure to make all the observation homogeneous in term of reference
196 systems was applied before conducting the network adjustment and then the roto-translation into
197 VRS (Figure 5).

198 In particular, the TS observations (angles and distances), referred to Local Reference Frame
199 (LRF) and the GNSS baselines, referred instead to a geocentric Cartesian system, were brought to a
200 common Eulerian Reference System (ERS) established with the origin in the Central Building,
201 choosing xy plane tangent to the local sphere with the y axis along the North direction.

202 Therefore, the GNSS coordinates were transformed from the adopted Cartesian geocentric
203 reference system (ITRF08) to the defined ERS by the analytical transformation:

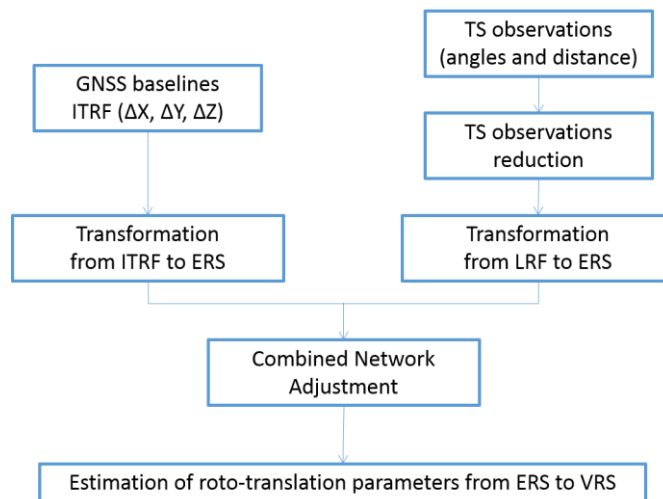
204
$$\mathbf{X}_{ERS} = R(\varphi_0, \lambda_0)(\mathbf{X} - \mathbf{X}_0) \tag{1}$$

205 setting the approximate ERS origin inside the central building (Table 3).

206 **Table 3.** Coordinates of the ERS origin

	φ_0	λ_0	H_0 (m)	X_0 (m)	Y_0 (m)	Z_0 (m)
Origin	10° 30' 16''	43° 37' 53''	9.0	4546337.287	842981.326	4378541.338

207

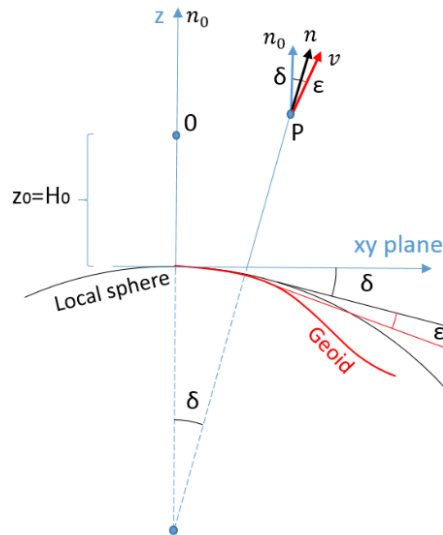


208

209 **Figure 5.** Scheme of GNSS and TS measurements integration and their alignment to VRS

210 The TS measurements were corrected according to the approach proposed by [13]. Due the
211 network extension, it was necessary to consider the terrestrial curvature: the network adjustment was
212 performed combining a spherical reference surface with a 3D Cartesian coordinate system, as shown
213 in Figure 6.

214



215

216

217

Figure 6. ERS and geodetic reference surface approximation: combined effects of vertical deflection (ϵ) and terrestrial curvature (δ).

218

219

220

221

222

223

224

225

226

227

228

229

230

231

232

233

234

235

236

237

238

In a generic point P , the direction of the vertical is rotated respect to the origin 0 of the ERS by the terrestrial curvature and by the variation of the vertical deflection. The least squares adjustment is possible by using the simple 3D Cartesian equation model, applying to the observations a set of correction factors. The correction for the terrestrial curvature was easily calculated by approximated coordinates: angle observations needed corrections ranging from 55^{cc} to 300^{cc} , considerably minor in the horizontal angles rather than on the vertical ones. Meanwhile, as stated in [13], the variation of the deviation of the vertical was neglected thanks to the short distances involved ($<10\text{km}$).

The least square network adjustment, performed with the scientific software CALGE [14], provided the best estimate of the coordinates including their precision.

The software requires as input a redundant number of observations to form the equations for each 3D ranges, azimuthal, zenithal angles and the ERS baseline components. Error models for GNSS baselines and accuracy defined according to the TS specifications were also adopted.

A preliminary computation has been performed using only the TS angular measurements in order to identify outliers before the final network adjustment that includes also GNSS baselines, as described in Figure 3 (green connections) in order to improve the geometry.

Considering that the distances between the surveyed points range between 5 m and 1500 m, the error model (weights) for the TS observations was defined as a function of the distance, in order to balance the effects of the collimation error for different distances. A sensitivity analysis to refine the overall error model was performed, providing the results reported in Table 4 and 5, for distance and angles respectively. The final adjustment provided results with standard deviation lower than 1 mm for the xy coordinates and lower than 1.5 mm for the z .

239

Table 4. A priori standard deviation for distance observations used in the network adjustment

Distance (m)	TM50		TDA5000	
	Fixed error (mm)	Proportional Error (ppm)	Fixed error (mm)	Proportional Error (ppm)
$<200\text{m}$	0.6	1	1	2
$\geq 200\text{m}$	1	1	1.5	2

240

241

Table 5. A priori standard deviation of angle observations used in the network adjustment

Distance (m)	TM50	TDA5000
--------------	------	---------

	Horizontal angle (grad)	Vertical angle (grad)	Horizontal angle (grad)	Vertical angle (grad)
<5	$2 \cdot 10^{-3}$	$3 \cdot 10^{-3}$	$2 \cdot 10^{-3}$	$3 \cdot 10^{-3}$
5-10	$1.5 \cdot 10^{-3}$	$2.5 \cdot 10^{-3}$	$1.5 \cdot 10^{-3}$	$2.5 \cdot 10^{-3}$
10-50	10^{-3}	$2 \cdot 10^{-3}$	10^{-3}	$2 \cdot 10^{-3}$
50-200	$0.8 \cdot 10^{-3}$	$1.5 \cdot 10^{-3}$	$0.8 \cdot 10^{-3}$	$1.5 \cdot 10^{-3}$
>200	$0.5 \cdot 10^{-3}$	10^{-3}	$0.5 \cdot 10^{-3}$	10^{-3}

242

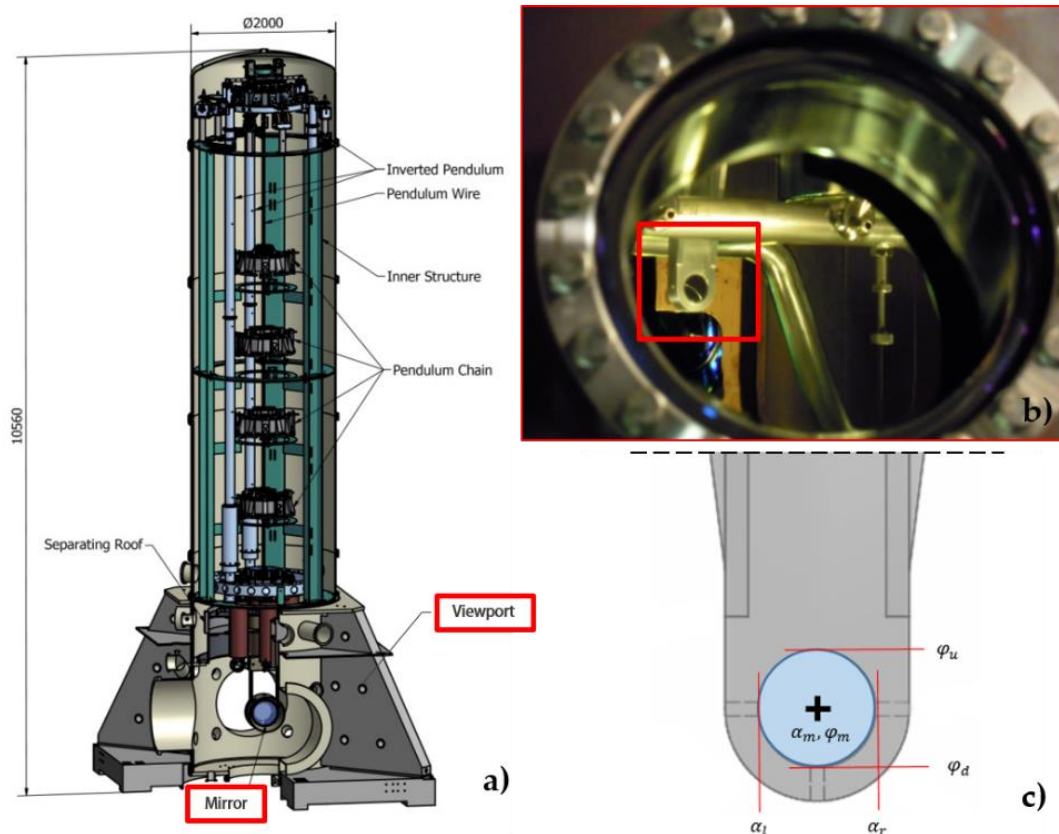
243 In order to express the network into the VRS reference system, the estimated ERS coordinates
 244 were clockwise rotated using the GPS00N-GPS10N baseline and translated to fix the origin by
 245 determining the shift parameters thanks to five points known also in the oldVRS.

246 **3. Georeferencing Virgo interferometer**

247 The establishment of the VRS reference frame and the determination of the transformation
 248 parameters between ITRF and VRS have also allowed the inverse transformation $VRS \rightarrow ITRF$ and
 249 the estimation of the ITRF coordinates of the Virgo Control Points (VCPs).

250 VCPs are the centres of the Beam Splitter (BS), North End (NE) and West End (WE) suspended
 251 mirrors: points fully defining the location and orientation of the Virgo interferometer respect to the
 252 other Gravitational Waves detectors (LIGO Hanford, WA, USA; LIGO Livingston, LA, USA; GEO,
 253 Germany; KAGRA, Japan), contemporary observing the Universe signals.

254 Mirrors are not accessible with a direct survey because they are located inside the vacuum
 255 enclosures at the ends of the interferometer arms (Figure 7). They are visible only across two
 256 viewports at the bottom of the pendulum towers, so the centre of each mirror was indirectly surveyed
 257 by TS, collimating the edges of the metallic mirror frame across the viewport glasses. Executing the
 258 survey from both the viewports, the space resection of the VCPs was realized only by means of TS
 259 angle observations.
 260



261

262
263
264

Figure 7. Suspended mirror of Virgo detector inside the Ultra-High Vacuum system: pendulum apparatus (a), mirror view through a viewport (b) and indirect determination of the mirror centre by external mirror edges collimation (c).

265
266
267
268

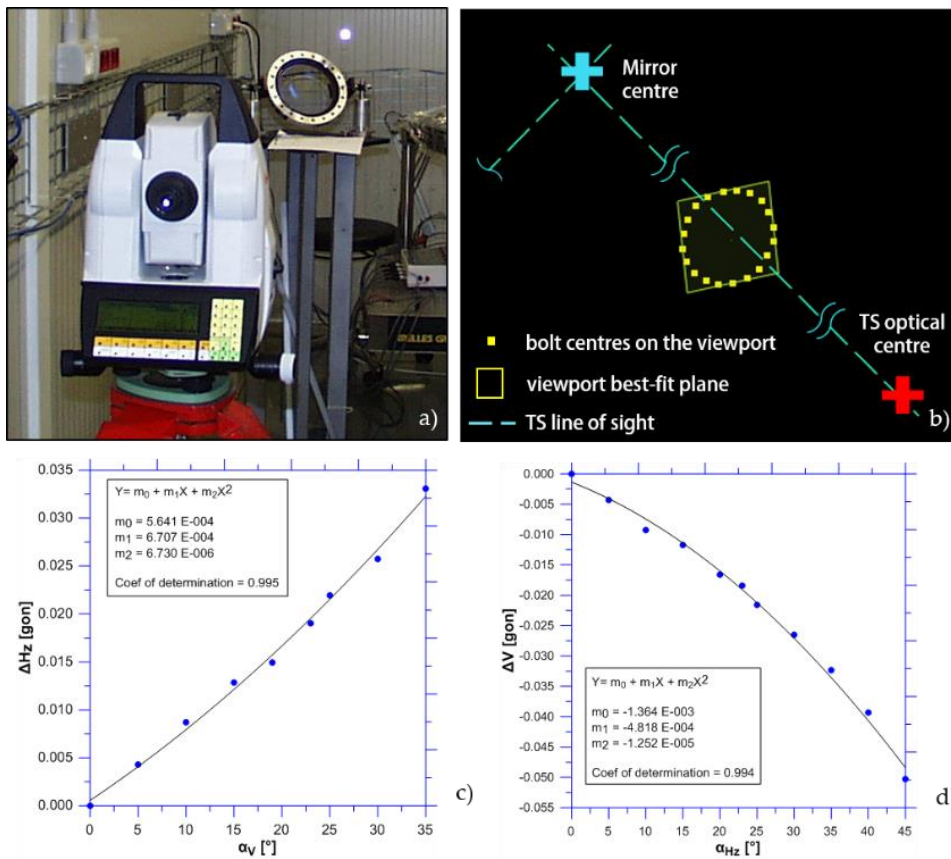
The effect of the glass optical refraction was investigated by means of angular measurements across a viewport with analogous optical and geometrical characteristics (figure 8): it was reconstructed the analytical model of the optical ray deviations, changing systematically the incidental angle of the TS line of sight.

269
270
271
272
273

The TS and mirror centres coordinates permit to define the line of sight directions. The glass plane attitude was reconstructed by means of a best-fit computation of the bolts centres, which fix the metallic frame of the viewports. The angular correction values corresponding to the estimates of the incident angles were applied to the TS observations in order to obtain a reliable set of coordinates for the mirrors centres.

274
275
276
277
278

The VRS coordinates of VCPs transformed into ITRF08 allowed also to determine the global alignment of the local network with respect to the North. The azimuth of the geodesic curve through BS and NE, with respect to the North, is $19^{\circ} 25' 58''.7265$. The azimuth of the geodesic curve through BS and WE, with respect to the North, is $289^{\circ} 25' 58''.5720$.



279

280
281
282
283

Figure 8. Experimental investigation about the effects of glass viewport crossing on angular observations: repetitions of TS measurements with different incident angles in laboratory (a), reconstruction of the incidental angle between the TS lines of sight and the glass plane during survey (b), analytical models of the ray deviations (c, d).

284

4. Soil settlement monitoring

285
286
287
288

The existence of a subsidence phenomenon in the area of the Virgo interferometer was well known since the early designing phase of the civil engineering works [15, 16]. Therefore, all the relevant infrastructures were designed considering this effect based on several geotechnical studies carried out considering the characteristics of the soil present in the area. Intensive geological surveys

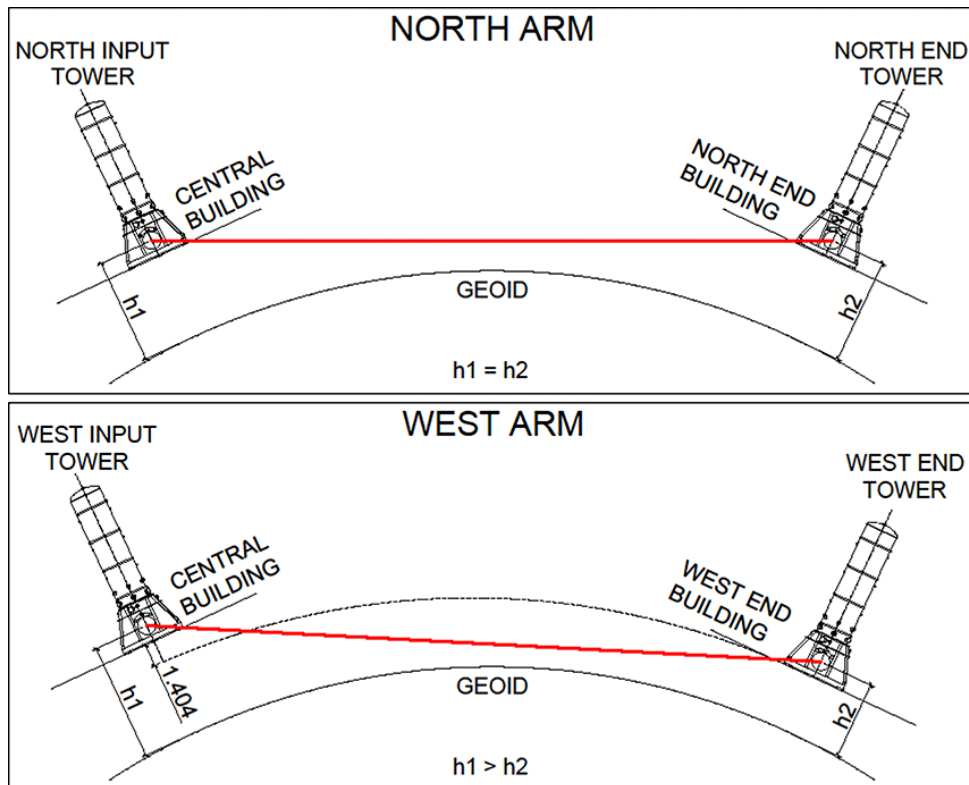
289 [17, 18] were performed in order properly define the soil characteristics and to model the expected
290 settlement pattern in response to the loads. Nevertheless, the need to monitor the displacements and
291 compare these with the expected values, as well the tight specifications set for hosting the Virgo
292 interferometer, have required a continuous surveying activity to control the position of the buildings.

293 The main monitoring activity at Virgo site is devoted to control the subsidence processes
294 activated in the area due to the overload of the constructions considering that there are two
295 fundamental conditions to be fulfilled:

- 296 • For optical requirements, the interferometer has to lay in a 3x3km plane (vertical displacement
297 less than 5 mm per month, less than 10 mm per year; less than 150 mm in 20 years) and the
298 tunnel axes have to be orthogonal with an accuracy of ± 0.02 mrad;
- 299 • The operation along the two 3km-long UHV tubes requires that relative settlement of any pipe
300 cross section is kept less than 5 mm compared to the previous survey, as limit of stress for the
301 vacuum tube welding.

302 At the design stage in 2001, in order to accomplish the morphology of the area, the topographic
303 height of the beam (suspended mirror centre) was set the same at Central and North End Buildings,
304 while a difference of -1.404 m was established between the Centrale and the West End Building
305 (Figure 9).

306



307

308 **Figure 9.** Schematic profiles of the two orthogonal 3km long arms forming the Virgo laser
309 interferometer, showing the initial offset of the End Buildings with respect the Central Building at the
310 start of the monitoring.

311 The monitoring consists of topographic measurements to check the differential displacements
312 between two adjacent modules (distance 15 m). In addition to the direct measurements, an
313 application of Differential Interferometry using Synthetic Aperture Radar (DInSAR) was performed
314 as described in the following paragraph.

315 Defining an accurate VRS is the technical prerequisite for the monitoring activities concerning
316 the relative positions of the different components of the interferometer. For the evaluation of relative
317 displacements, every sets of measurements carried out over the years has been reduced in the VRS

318 relative reference system with respect to the optical centre of the interferometer, located in the Central
319 Building.

320 4.1. Topographic monitoring

321 Since 2001 over 500 internal reference points and 30 external concrete pillars of VRS network
322 were periodically measured. Realignment procedures have to be carried out when the relative
323 displacement between two modules exceeds a threshold of 5 mm, from previous survey. The
324 threshold is lowered to 2 mm for the special modules attached to the large vacuum tube valves, close
325 to the experimental buildings (Figure 10).



326

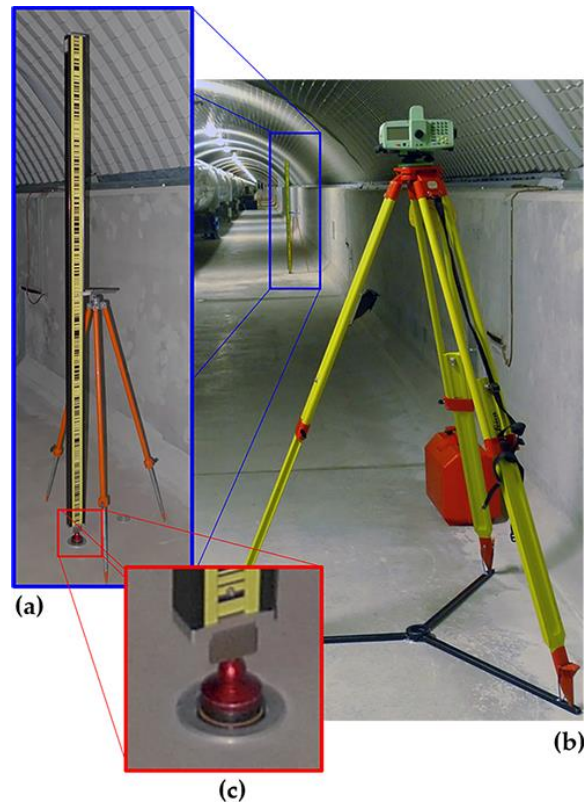
327 **Figure 10.** End Building-Tunnel link module. Special tube support with micrometric mechanical
328 realignment system.

329 The monitoring measurements along both tunnels (West and North Arms), carried out since
330 2001, include high-precision levelling and GPS surveys. Being the main purpose, the evaluation of
331 the relative displacements referred to the optical centre of the interferometer, all surveys have been
332 reduced to the zero points located in the Central Building. Also, the mutual position of these two
333 main reference points has been checked by periodic accurate levelling, in order to observe the whole
334 evolution of the interferometer.

335 Periodically, GPS measurements in combination with TS measurement to monitor horizontal
336 displacement while leveling for vertical displacement were realized to check horizontal
337 displacements. In order to maintain the expected accuracy requirements, the following conditions
338 were adopted (figure 11):

- 339 • Inter-distance of 15 m between the benchmarks along the tunnels;
- 340 • Reference points materialized by accurate centring system;
- 341 • Staff positioned with tripod on each point;
- 342 • Similar environmental conditions (temperature and relative humidity);
- 343 • Not significant air flows in the tunnels;
- 344 • Same tolerances adopted for the setup of the instruments.

345 The instruments adopted are the TS Leica TDA5000 for the initial survey, optical level Leica
346 NA2+ GPM3 for the first levelling, and digital level Leica DNA03 since 2003 to now. The frequency
347 of the measurement campaigns has been gradually decreased over the years from the initial 6 months
348 up to 24 months, in function of the soil settling.



349

350 **Figure 11.** High precision equipment adopted for the levelling along the tunnels: a) Leica DNA03
 351 station, b) rod on a reference point set by tripod and c) accurate 3D centring system of reference points
 352 placed on the tunnel floor.

353 The main levelling parameters are summarized in the following Table 6, which also reports the
 354 max e min error of closure obtained among the whole measurement campaigns.

355

Table 6. Summary of levelling parameters.

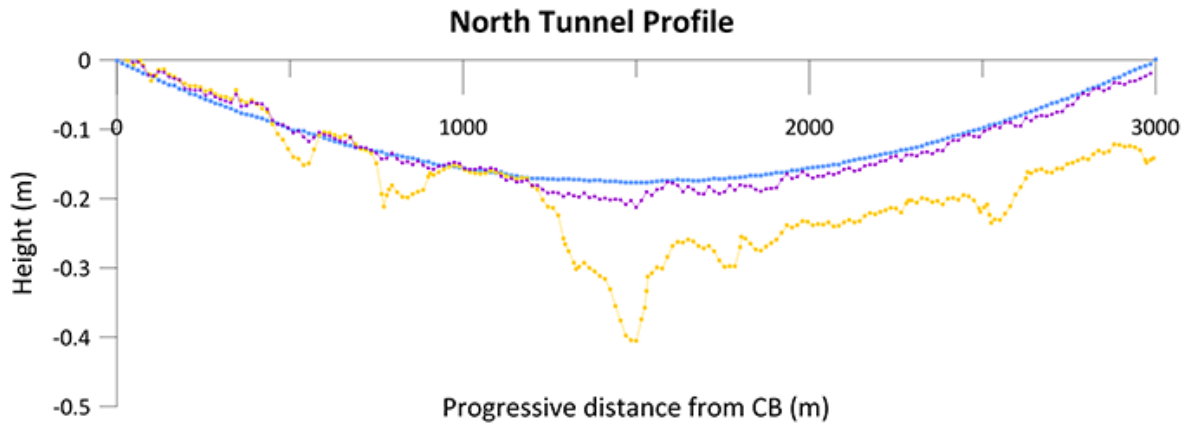
Line length	Number of stations	Max closure error	Min closure error	Max closure error	Min closure error
3006 m /line	205 /line	4.42 mm	3.76 mm	1.26 mm	0.03 mm

356

357 4.2. Settlement data analysis and results

358 The monitoring activity revealed since 2002 a steady subsidence process over the years because
 359 of the building and embankment overloads.

360 The following Figures 12 and 13 show trend diagrams of elevation components, where last
 361 survey of the tunnel profile is compared with the theoretical design position and the tube axis profile
 362 effectively realigned, sum of the operations since the start of the realignment process. Note that in
 363 such diagrams the x-coordinate represents the progressive distance from the Central Building as
 364 rectified geoid.
 365



366

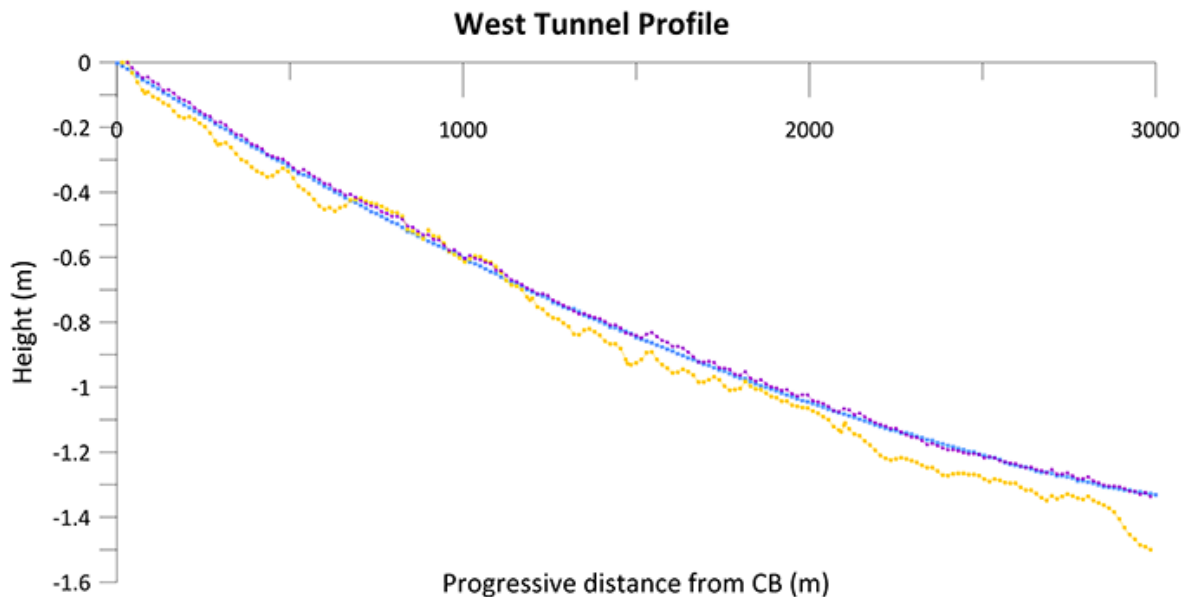
367

368

369

Figure 12. North Tunnel Profile: theoretical tracking curve (light blue); cumulated displacements at Feb 2017 (yellow); realigned profile made by the sum of the realignment activities over years 2003-2017 (purple).

370



371

372

373

374

Figure 13. West Tunnel Profile: theoretical tracking curve (light blue); cumulated displacement at Jan 2017 (yellow); realigned profile made by the sum of the realignment activities over years 2003-2017 (purple).

375

376

377

378

379

380

381

382

Analysing the data collected during the years it is possible to foresee an evolutive scenario of the phenomenon. A best-fitting curve analysis was performed on the tunnel areas showing the most pronounced effects. Particularly, these are located in the middle part of the North Tunnel (reference points N100) and in the zone of the West Tunnel next to the West End Building (reference points W199 and W200). These locations are not surprising, since those areas were interested by the major embankment overloads for the construction of the adjacent buildings. Indeed, most important settlements of the tunnels have been surveyed in correspondence of overloads on soil, related to civil works.

383

384

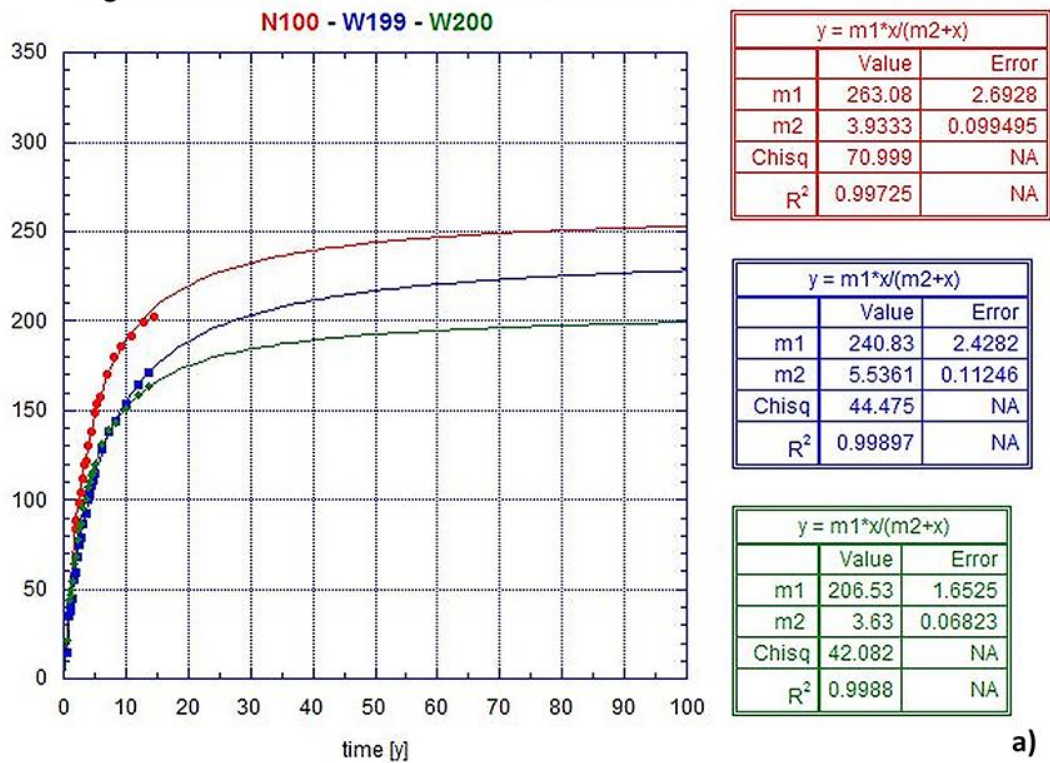
385

386

Several types of fitting curves were considered and, among them, the "Michaelis-Menton" law or the logarithmic law of order 2 provided the highest value of the coefficient of determination R^2 . The first curves are more coherent with the empirical formulas available in geotechnical literature.

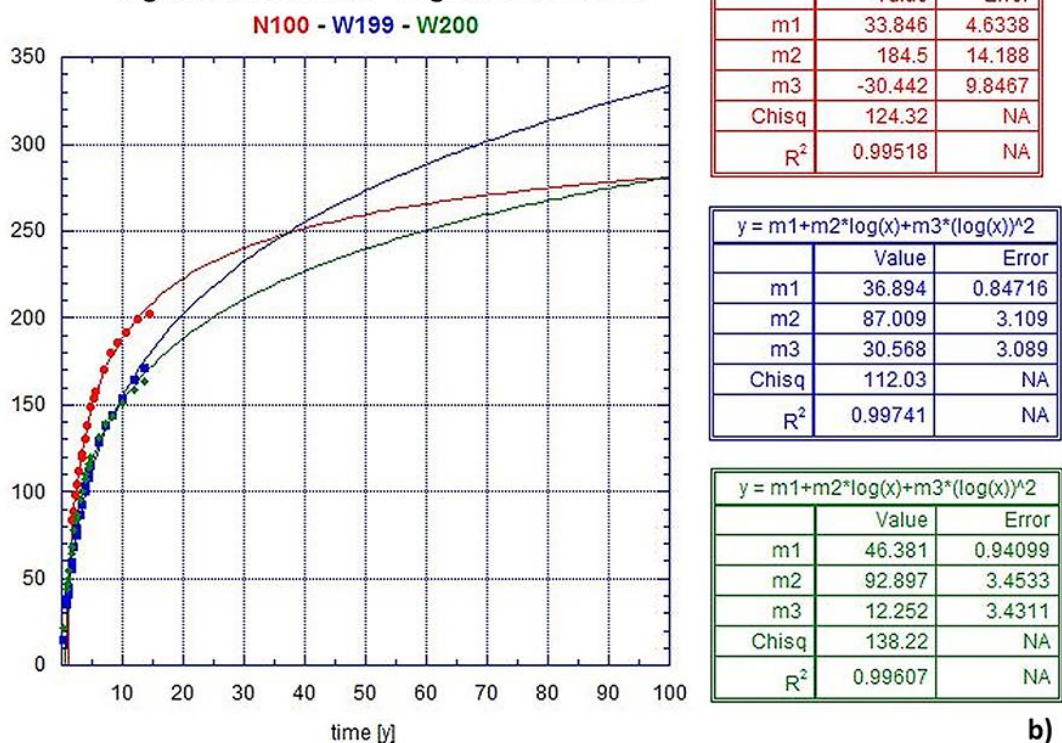
Figure 14 shows the diagrams for a projection over 100 years (to be considered as $t=\infty$).

Highest settlements - Michaelis-Menton curves



387

Highest settlements - Logarithmic curves



388

389

390

Figure 14. Best curve fitting for the highest settlements (N100-W199-W200). (a) “Michaelis-Menton” curves; (b) logarithmic curves (software KaleidaGraph by Synergy Software).

391

392

393

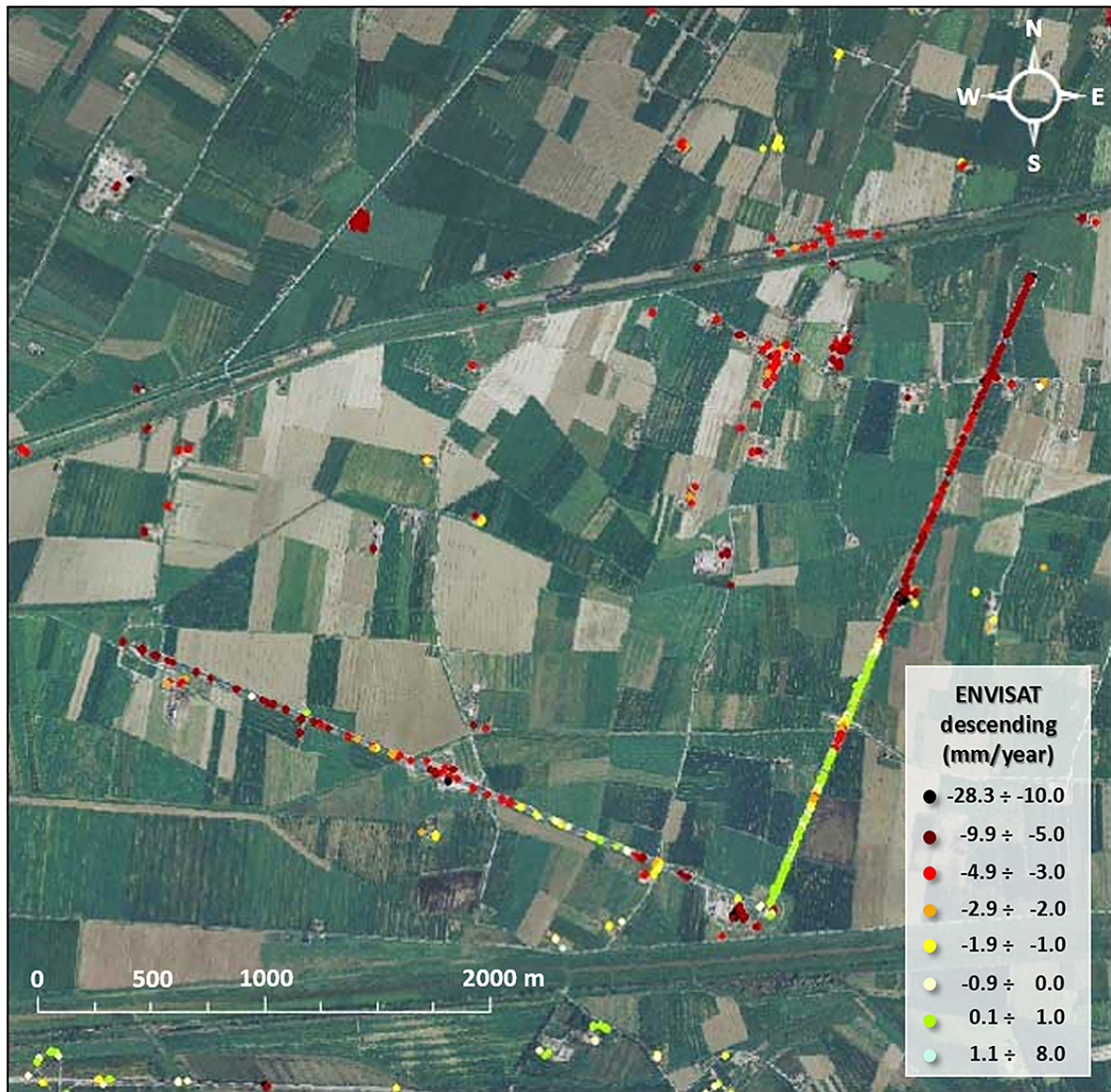
The analysis indicates that, although realignments will continue over a very long time period, the expected subsidence ($t=\infty$) is anyhow compatible with the realignment system (i.e. the length of the adjustable feet of the tube supports) and the space available inside the tunnel.

394 Clearly, these “a posteriori” hypotheses are related only to the surveyed data and focused on
395 own conditions of the Virgo tunnels and cannot be generalized. Moreover, the previous
396 considerations are based on the hypotheses that external factors will remain constant over time (i.e.
397 no large variations of the water deep stratum height in the area or new overloading of adjoining soil
398 close to the tunnels).

399 *4.3. DInSAR time series analysis and results*

400 Differential Synthetic Aperture Radar Interferometry (DInSAR) [19] is a technique based on
401 remote sensing data able to detect ground displacements. It relies on the processing of the phase
402 difference between two temporally separated SAR images. In particular, advanced DInSAR
403 approaches [20, 21] are based on the processing of SAR acquisition sequences collected over large
404 time spans to generate displacement time series of persistent scatters, that represents “targets” on the
405 surface that are able naturally to reflect radar signal (such as structures, infrastructures, etc.) without
406 the need of accessing to the site. The accuracy of DInSAR technique is estimated about centimetre to
407 millimetre [22].

408 Long-term DInSAR deformation time series have demonstrated the capability to provide
409 valuable information on the displacements that affect built up area [23, 24]. The DInSAR analysis was
410 performed to carry out an a-posteriori check on the subsidence process observed using ground-based
411 periodic surveying (levelling). Considering the level of agreement with the leveling and the capacity
412 of the DInSAR technique to measure displacement in absence of control points along the whole
413 structure and in the surrounding, it may be added to the routine monitoring schedule. This activity
414 will permit to more clearly identify the movements due to the structural overloading. Therefore, in
415 this paper was adopted this technique with the double aim: first to understand the overall settlement
416 affecting the area surrounding the Virgo interferometer and secondly to verify its performances
417 compared with classical levelling technique.
418



419

420

421

422

Figure 15. Displacement rates (mm/year) obtained applying DInSAR technique on VIRGO infrastructures and its surrounding area. The colour dots range from dark red (up to a velocity of -10mm/year) to stable points indicated in green.

423

424

425

426

DInSAR time series (acquired from Ministry of Environment and Protection of Land and Sea), obtained using a Permanent Scattering (PS) approach to process ascending and descending orbit data from ENVISAT satellite. The analysis was carried out on about 70 scenes collected on each orbit from January 2003 to June 2010.

427

428

429

430

431

432

433

434

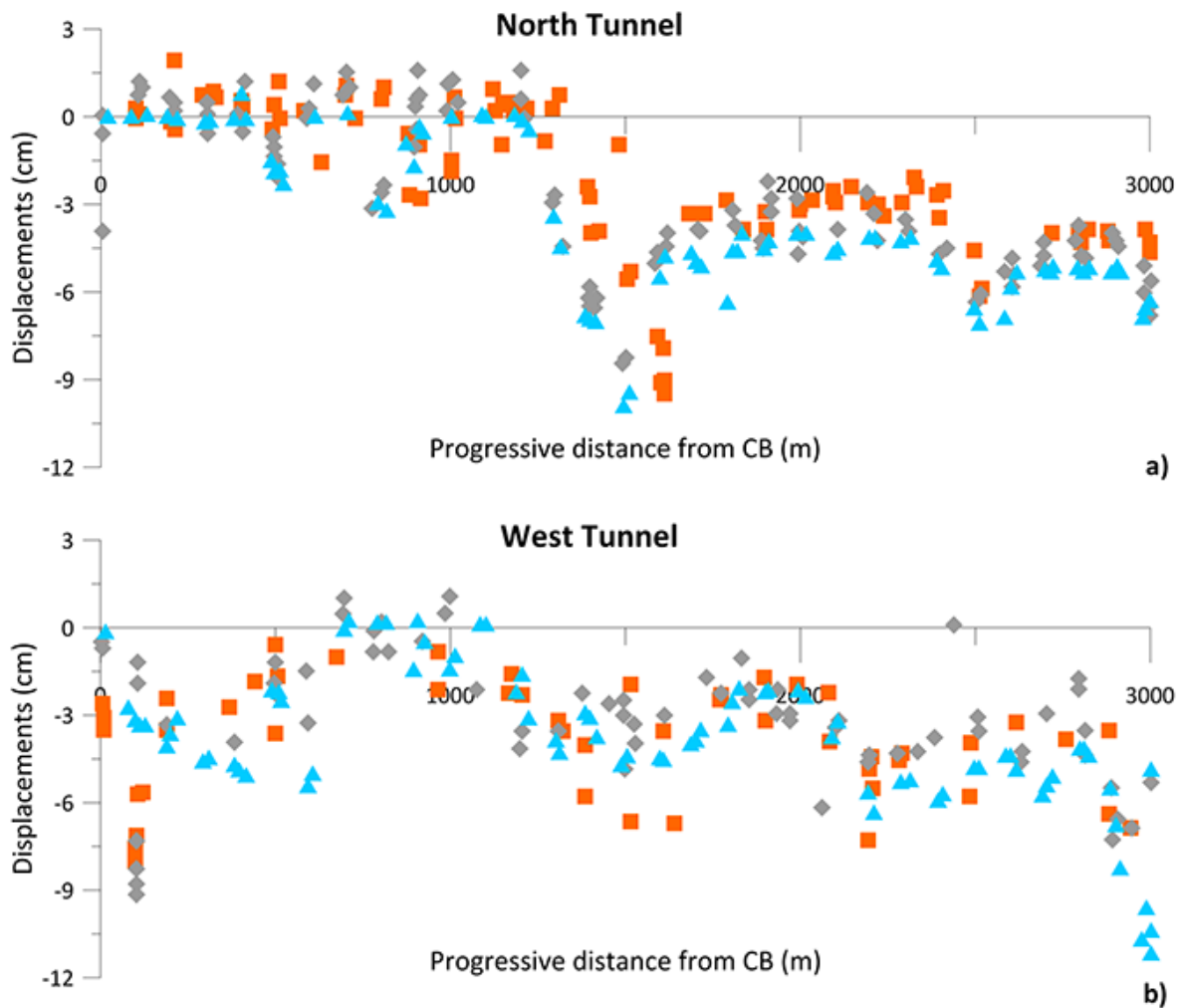
435

436

437

Figure 15 shows an overall view of the descending orbit result where colour scale dots indicates stable area (in green) and unstable area characterized by subsidence phenomena (in red). The DInSAR cumulative displacements along the North and West tunnels were compared with levelling data. Figure 16 shows the cumulated displacement of the whole 2003-2010 Envisat observation period, contemporary to the levelling sessions. These are obtained by selecting the DInSAR displacement extracted from SAR data acquired in days as much as possible close to the levelling surveying sessions. For both tunnels, the two different techniques revealed comparable subsidence trend. The displacements derived by the DInSAR data, although less accurate than the levelling ones, are characterized by larger ground coverage that allows to assess the ground subsidence phenomena at large scale. In fact, the study area is located within the Pisa alluvial plain characterized by clays and silts formations with layers of sands, peat and localized organic levels [25],

438 where the natural consolidation processes can be accelerated by overloads at the surface. DInSAR
439 data are useful to distinguish the subsidence linked to effects of the Virgo structures.
440



441
442
443 **Figure 16.** Comparison between levelling (in blue) and DInSAR data for ascending (in orange) and
444 descending (in grey) Envisat components along North Tunnel (a) and West Tunnel (b).

445 5. Conclusions

446 The construction and management of a difficult research infrastructure such as Virgo demands
447 high-precision geodetic surveying for the positioning of the instrumental parts. Besides, the extreme
448 sensitivity of the scientific facilities requires the implementation of regular monitoring to control the
449 displacements elapsing in time among the different parts of the interferometer, especially when the
450 site geotechnical setting is difficult such as at the Virgo site. Therefore, the high accuracy
451 requirements combined with the weak network geometry and the size of the connections implied the
452 integration of different techniques, based both on ground and space sensors.

453 Concerning the establishment of a local Reference System, the VRS, the integration of high
454 precision total stations and geodetic GNSS receivers offered the advantage to enforce the robustness
455 of the geodetic reference network. In particular, the use of GNSS allowed the link between the
456 terminal parts of the two tunnels of the interferometer, not mutually measurable with optical
457 instruments. Since the Virgo Control Points (VCPs) centres of the suspended mirrors were not
458 accessible, their connection to the VRS was possible only considering directions after having
459 modelled the refraction effect. This aspect suggests that future development should include further
460 systems to allow a direct measurement both to fully include them into the overall geodetic networks
461 and, eventually, to perform calibration tests.

462 A further relevant aspect has been the determination of the accurate geographic position of Virgo
463 respect to the other interferometers of the GW detector network, which is, in fact, fundamental for
464 the contemporary detection of signals coming from the Universe. The accuracy obtained for both the
465 VRS network points coordinates satisfies the initial specifications, considering the used instruments
466 and the adopted surveying methodologies.

467 Regular campaigns of high-accuracy levelling measurements integrated by GPS and theodolite
468 observations for the horizontal displacements permitted to quantify the evolution of the relevant and
469 expected subsidence process induced by the overloads of the Virgo structures acting on compressible
470 soils at foundation. In order to understand the overall settlement process, the evaluation of the
471 deformation patter of the Virgo area has been performed also through the DInSAR technique. The
472 comparison between the subsidence evaluated using DInSAR analyses and the direct measurement
473 by levelling provided a significant coherence in the evaluation of the general trend along the tunnels.
474

475 **Author Contributions:**

476

477 M.M. Surveying, data processing and analysis, paper writing.

478 C.N. Data processing and analysis, paper writing.

479 A.P. GNSS surveys, TS surveys, TS data processing and analysis, paper writing.

480 M.A.T. TS surveys, TS data processing and analysis, paper writing.

481 L.V. TS and GNSS surveys designing, TS and GNSS surveys, data analysis, paper writing.

482 A.Z. GNSS surveys, GNSS data processing and analysis, paper writing.

483

484 **Acknowledgments**

485

486 The authors thanks Ing. Alberico Sonnessa, Ing. Peppe J. V. D'Aranno and Dott. José A. Palenzuela
487 Baena for their contribution to the surveying activity. We are also grateful to Ing. Chiara Volante
488 that carried out the post-analysis of DInSAR data in comparison with the levelling one for her
489 master thesis dissertation.

490 DInSAR data were acquired from the Ministry of Environment and Protection of Land and Sea
491 (pcn.minambiente.it/mattm)

492 **Conflicts of Interest:** The authors declare no conflict of interest.

493 **References**

- 494 1. Virgo Collaboration. Advanced Virgo Technical Design Report. VIR-0128-12, EGO TDS, April 2012.
- 495 2. B. P. Abbott, et al. (LIGO Scientific Collaboration and VIRGO Collaboration). Observation of
496 Gravitational Waves from a Binary Black Hole Merger. *Phys. Rev. Lett.*, 116 (2016), 061102.
- 497 3. B. P. Abbott, et al. GW170817: Observation of Gravitational Waves from a Binary Neutron Star Inspiral.
498 *Phys. Rev. Lett.*, 119 (2017), 161101.
- 499 4. M. Masuzawa, T. Adachi, H. Iinuma, T. Kawamoto, Y. Ohsawa. SuperKEKB Main Ring Tunnel
500 Motion. in International Workshop on Accelerator Alignment 2014 (IWAA14), IHEP, Beijing, China,
501 October 2014.
- 502 5. D. Missiaen, M. Duquenne. Could the AT401 replace digital levelling and "Ecartometry" for the
503 smoothing and realignment of LHC. in International Workshop on Accelerator Alignment 2012
504 (IWAA14), Fermilab, Batavia, USA, September 2012.
- 505 6. J. Volk, V. Shiltsev, A. Chupyra, M. Kondaurov, S. Singatulin, D. Fratta, A. Meulemans, C. Potier, H.
506 Wang. Hydrostatic Level Systems at Fermilab and SURF. International Workshop on Accelerator
507 Alignment 2014 (IWAA14), Fermilab, Batavia, USA, September 2012.

- 508
509
510
511
512
513
514
515
516
517
518
519
520
521
522
523
524
525
526
527
528
529
530
531
532
533
534
535
536
537
538
539
540
541
542
543
544
545
546
547
548
549
550
7. D. Missiaen, T. Dobers, M. Jones, C. Podevin, J.P. Quesnel. The final alignment of the LHC. International Workshop on Accelerator Alignment 2008 (IWAA08), Tsukuba, Japan, February 2008.
 8. D. Missiaen, P. Dewitte, J.F. Fuchs, H. Mainaud Durand, T. Dobers, M. Jones, J.C. Status report of projects activities at CERN. International Workshop on Accelerator Alignment 2014 (IWAA14), IHEP, Beijing, China, October 2014.
 9. B. O'Sheg Oshinowo, H. Friedsam. Survey of the NOvA Near Detector at Fermilab. International Workshop on Accelerator Alignment 2010 (IWAA10), DESY Hamburg, Germany, September 2010.
 10. R. Beunard, A. Lefevre, F. Legruel. The Initial Geodetic Survey for the SPIRAL2 Process Installation. International Workshop on Accelerator Alignment 2010 (IWAA10), DESY Hamburg, Germany, September 2010.
 11. S. Matsui, H. Kimura, Survey Comparison using GNSS and ME5000 for One kilometer Range. International Workshop on Accelerator Alignment 2008 (IWAA08), Tsukuba, Japan, February 2008.
 12. R. Dach, S. Lutz, P. Walser, P. Fridez. Bernese GNSS Software Version 5.2. User Manual. Astronomical Institute, University of Bern, 2015, Bern Open Publishing <http://dx.doi.org/10.7892/boris.72297>.
 13. Brovelli M.; Sansò F., Equazioni di osservazione della topografia in coordinate cartesiane locali: scrittura, linearizzazione e analisi dei relativi ambiti di validità, Boll. Di Geod. E Sci. Affin. 3 (1989) 255–274, (in Italian).
 14. Forlani, G. Sperimentazione del nuovo programma CALGE dell'ITM. Boll. SIFET 2 (1986), (in Italian).
 15. Virgo Collaboration. Feasibility Study of the civil works of the Virgo Project EGO TDS, April 1994.
 16. Virgo Collaboration. Study of the Land subsidence of Pisa plain south the Arno river. EGO TDS, December 1994.
 17. Virgo Collaboration. First Geological Survey of the Virgo Project Area. EGO TDS, July 1991.
 18. Virgo Collaboration Second Geological Survey of the Virgo Project Area. EGO TDS, September 1994.
 19. A.K. Gabriel, R.M. Goldstein, H.A. Zebker. Mapping small elevation changes over large areas: differential interferometry, Jour. Geophy. Res., 94 (1989), 9183–9191 DOI: 10.1029/JB094iB07p09183
 20. A. Ferretti, C. Prati, F. Rocca. Non-linear subsidence rate estimation using permanent scatters in Differential SAR Interferometry, IEEE Trans. Geosci. Remote Sens., 38 (2000). DOI: 10.1109/36.868878.
 21. R. Lanari, O. Mora, M. Manunta, J.J. Mallorquí, P. Berardino, E. Sansosti. A small baseline approach for investigating deformations on full resolution differential SAR interferograms. IEEE Trans. Geosci. Remote Sens., 42 (2004), DOI: 10.1109/TGRS.2004.828196.
 22. F. Casu, M. Manzo, R. Lanari. A quantitative assessment of the SBAS algorithm performance for surface deformation retrieval from DInSAR data. Remote Sens. Environ. 102 (2006), 3-4, DOI: 10.1016/j.rse.2006.01.023.
 23. M. Bonano, M. Manunta, M. Marsella, R. Lanari. Longterm ERS/ENVISAT deformation time-series generation at full spatial resolution via the extended SBAS technique, Int. J. Remote Sens., 33 (2012), 15, DOI: 10.1080/01431161.2011.638340.
 24. S. Scifoni, M. Bonano, M. Marsella, A. Sonnessa, V. Tagliafierro, M. Manunta, R. Lanari, C. Ojha, M. Sciotti. On the joint exploitation of long-term DInSAR time series and geological information for the investigation of ground settlements in the town of Roma (Italy). Remote Sens. Environ., 182 (2016), DOI: 10.1016/j.rse.2016.04.017.
 25. G. Sarti, V. Rossi, A. Amorosi. Influence of Holocene stratigraphic architecture on ground surface settlements: A case study from the City of Pisa (Tuscany, Italy). Sediment. Geol.. 281 (2012), DOI: 10.1016/j.sedgeo.2012.08.008 .